Contents lists available at ScienceDirect

Neoplasia

journal homepage: www.elsevier.com/locate/neo

Original Research

Tumor neoantigens as key drivers of significant anti - tumor immunity in triple - negative breast cancer mouse models

Yujeong Her [a,1], Jeong Yeon Kim [b,c,1], Hocheol Shin [d,e], Kwangmin Yu [f], Kyu-Jin Lee [a], Yi Rang Na [f,g,h], Sangyong Jon [d,e,*], Jung Kyoon Choi [b,c,*], Hyeong-Gon Moon [i,j,k,l,*]

[a] Interdisciplinary Program in Cancer Biology, Seoul National University College of Medicine, Seoul, Republic of Korea
[b] Department of Bio and Brain Engineering, KAIST, Daejeon, Republic of Korea
[c] Penta Medix Co., Ltd., Seongnam, Republic of Korea
[d] Department of Biological Sciences, KAIST Institute for the BioCentury, Korea Advanced Institute of Science and Technology (KAIST), Daejeon, Republic of Korea
[e] Center for Precision Bio-Nanomedicine, Korea Advanced Institute of Science and Technology (KAIST), Daejeon, Republic of Korea
[f] Immunology Core Facility, Biomedical Research Institute, Seoul National University Hospital, Seoul, Republic of Korea
[g] Translational Immunology Lab, Department of Transdisciplinary Medicine, Seoul National University Hospital, Seoul 03080, Republic of Korea
[h] Department of Biomedical Sciences, Seoul National University College of Medicine, Seoul 03080, Republic of Korea
[i] Department of Surgery, Seoul National University Hospital, Seoul, Republic of Korea
[j] Department of Surgery, Seoul National University College of Medicine, Seoul, Republic of Korea
[k] Genomic Medicine Institute, Medical Research Center, Seoul National University, Seoul, Republic of Korea
[l] Cancer Research Institute, Seoul National University, Seoul, Republic of Korea

ARTICLE INFO

Keywords:
Neoantigen
Immunotherapy
Triple negative Breast cancer
Tumor immune microenvironment
Checkpoint blockade
Lipid nanoparticle
T cell

ABSTRACT

Recent studies have highlighted the therapeutic potential of targeting tumor neoantigens in solid tumors; however, its efficacy in breast cancer remains unclear. Here, we evaluate the impact of tumor neoantigen-targeted strategies in a syngeneic mouse mammary carcinoma model. Mice previously exposed to 4T1 tumor cells (PETCs) or treated with tumor cell-derived lysates (TdLs) exhibited robust antitumor immunity, leading to reduced tumor growth and metastasis through tumor immune microenvironment remodeling. TdL administration in mice harboring orthotopic tumors significantly enhanced the efficacy of immune checkpoint blockade, suggesting its potential as an immunotherapeutic adjuvant. To further optimize neoantigen-based approaches, we developed a lipid nanoparticle (LNP)-based delivery system for neoantigen peptides, which effectively suppressed tumor progression and metastasis in vivo. Mechanistically, this strategy promoted antigen-specific T cell activation and reshaped the tumor immune landscape, enhancing immune-mediated tumor rejection. These findings underscore the therapeutic promise of personalized tumor neoantigen-targeted immunotherapy in breast cancer and support its further evaluation in clinical settings.

Introduction

Human breast carcinomas constitute a diverse array of tumors, displaying heterogeneity in behavior, prognosis, and treatment response. While the incidence of breast cancer remains substantial, advances in therapy have led to a decrease in overall mortality rates [1]. Over the past decade, the landscape of cancer therapy has undergone a transformative shift with the advent of immunotherapy, a revolutionary approach targeting the immune system [2]. Immunotherapy, particularly immune checkpoint inhibitors (ICIs), has become the established standard of care for various solid tumor types, significantly enhancing clinical outcomes [3,4]. However, despite the success of ICIs across a range of cancers, breast cancer patients exhibit limited responsiveness to these therapies [5–7], highlighting the need for a deeper understanding of the underlying mechanisms governing immune response dynamics within the tumor microenvironment (TME).

Recent studies have highlighted the roles of tumor-specific antigens (TSAs) or neoantigens in driving antitumor immune responses in solid

* Correspondence authors.
E-mail addresses: syjon@kaist.ac.kr (S. Jon), jungkyoon@kaist.ac.kr (J.K. Choi), moonhg74@snu.ar.kr (H.-G. Moon).
[1] These authors contributed equally: Yujeong Her, Jeong Yeon Kim.

https://doi.org/10.1016/j.neo.2025.101205
Received 2 April 2025; Accepted 23 June 2025

tumors [8–11]. In particular, efforts have been made to harness individual tumor neoantigens to establish an effective personalized immunotherapeutic strategy that can eradicate residual tumor cells and prevent metastasis across various cancer types [12–15]. In the TME, TSAs expressed by professional antigen-presenting cells (APCs) trigger the activation of antigen-specific T cells [16,17]. APCs display the full complement of necessary costimulatory molecules, which are essential for initiating antitumor immunity. The sustained expression of these costimulatory molecules, combined with the remarkable antigen-presenting abilities of dendritic cells via MHC class I molecules to $CD8^+$ T cells, plays a crucial role in shaping an effective antitumor immune response to solid tumors [18–20].

In this study, we investigated the potential value of novel immunotherapeutic approaches that can modulate antitumor immunity by remodeling the tumor immune microenvironment (TIME). Specifically, we tested the efficacy of various methods of delivering tumor-specific neoantigens in syngeneic mouse mammary carcinoma models and elucidated the mechanisms involved. Our data demonstrate the possibility that tumor neoantigen delivery can provide a novel effective immunotherapeutic strategy for triple-negative breast cancer.

Methods

Cell lines

4T1 (mammary carcinoma) and EMT6 (mammary carcinoma) cells were purchased from American Type Culture Collection (ATCC, VA, USA). RENCA (adenocarcinoma) and CT26 (colon carcinoma) cells were purchased from the Korean Cell Line Bank (KCLB, Seoul, South Korea). All the cell lines were cultured in complete growth medium containing RPMI-1640 (Welgene, Seoul, South Korea). To prepare this medium, fetal bovine serum (Welgene) and penicillin–streptomycin solution (Gibco, Waltham, MA, USA) were added to the base medium, reaching final concentrations of 10% and 1%, respectively. The cells were maintained in a 37°C incubator with 5% CO2 under humidified conditions.

Animals

Five-week-old female BALB/c mice were purchased from Korean Animal Technology (KOATECH, Gyeonggi, South Korea). All procedures received approval from the Association for the Assessment and Accreditation of Laboratory Animal Care. The animal care and use protocol was reviewed and approved by the Institutional Animal Care and Use Committee of Seoul National University Hospital (no. 23-0249-S1A0). The animals were housed in a facility accredited by AAALAC International (#001169) and maintained in accordance with the Guide for the Care and Use of Laboratory Animals 8th edition, NRC (2010).

Tumor-derived lysate (TdL) procedure

4T1 cells that had adhered to the cell culture dish were incubated at 42°C for 1 hour and then incubated at 37°C for 2 hours. The cells were subsequently harvested and transferred at a concentration of 1×10^6 cells/100 μl/mouse in Dulbecco's phosphate-buffered saline (DPBS) (Welgene) into 1.5 ml microcentrifuge tubes (Merck, Darmstadt, Germany). The cells underwent five repetitive freeze–thaw cycles, and the TdL stocks were frozen at −80°C for later in vivo application.

Selection and synthesis of 4T1 neoantigen peptides

To identify candidate neoantigens expected to exert anticancer effects, we employed a multiomics approach. First, cancer-specific somatic mutations were identified with whole-exome sequencing. The raw sequencing data were aligned to mouse reference genome using Burrows-Wheeler Aligner (http://bio-bwa.sourceforge.net) version 0.7.17. Then, we removed duplicate reads with Picard version2.26.6 and performed base quality score recalibration (BQSR) using Genome Analysis Toolkit version4.1. Somatic mutations were identified with MuTect2 using matched normal sequencing data to ensure cancer specificity. These mutations were further filtered on the basis of depth (>10) and variant allele frequency (>0.1). The protein sequences affected by these somatic mutations were then retrieved and analyzed using Variant Effect Predictor (v.104) and pVAC-seq (v4.0.10). Moreover, to ensure expression of genes harboring somatic mutations, we also conducted bulk RNA sequencing. The raw data were aligned to mouse reference genome using STAR v2.7.3 and transcriptome quantification was performed with HTSeq version2.0.1. We selected genes with TPM > 1 to ensure expression. The immunogenicity of peptides arising from mutant proteins was predicted using DeepNeo, an algorithm that predicts not only peptide–MHC binding but also T cell receptor responses to peptide–MHC pairs. [ref] (Kim, J.Y., et al., MHC II immunogenicity shapes the neoepitope landscape in human tumors. Nature Genetics, 2023. 55(2): p. 221-231.). To maximize anti-tumor effect, we prioritized candidate neoantigens, with preference of neoantigens predicted to react with multiple MHC genotypes including both the MHCI ($CD8^+$T response) and MHCII ($CD4^+$T response) contexts. Finally, single-cell RNA sequencing was used to calculate the frequency of cells expressing genes harboring candidate peptides. Additionally, peptide characteristics such as hydrophobicity, polarity, and instability were considered to facilitate peptide production. The information regarding our selected peptides for lipid nanoparticles (LNPs) is provided in Fig. S Table 2.

Preparation of neoantigen peptide-loaded lipid nanoparticles (LNPs)

Monoarginine-cholesterol (MA-Chol) and neoantigen peptide-loaded LNPs were prepared as previously described with a minor modification [refs] (Kim, Y.; Kang, S.; Shin, H.; Kim, T.; Yu, B.; Kim, J.; Yoo, D.; Jon, S., Sequential and Timely Combination of a Cancer Nanovaccine with Immune Checkpoint Blockade Effectively Inhibits Tumor Growth and Relapse. *Angew Chem Int Ed Engl* **2020,** *59* (34), 14628-14638.; Shin H, Kim Y and Jon S*, "Nanovaccine displaying immunodominant T cell epitopes of fibroblast activating protein is effective against desmoplastic tumors", ACS Nano 2023; 17, 10337-10352.). Cysteinylated neoantigen peptide, CKLWRYSYTA or CYFRNVDYLL, was conjugated to DSPE-PEG_{2000}-PDP via a disulfide exchange reaction. The two components were dissolved and mixed in dimethyl sulfoxide at a molar ratio of 1:2, followed by gentle vortexing at room temperature overnight. The reaction was halted by the addition of acetonitrile, and the DSPE-PEG_{2000}-neoantigen peptide conjugate was purified by high-performance liquid chromatography (HPLC) and characterized by matrix-assisted laser desorption/ionization-time of flight (MALDI-TOF) spectrometry. Neoantigen peptide-loaded LNPs were prepared, comprising MA-Chol:DOPE:DSPE-PEG_{1000}:DSPE-PEG_{2000}-neoantigen peptide at a molar ratio of 48.625:48.625:2.25:0.5, were prepared via thin-film formation and rehydration methods. Lipid components dissolved in chloroform and methanol were dried, followed by rehydration with HEPES-buffered glucose (HBG) containing CpG ODN. The solution underwent sonication, stirring, and extrusion, resulting in the encapsulation of CpG ODN. For characterization, the hydrodynamic size of the neoantigen peptide-loaded LNPs was determined by dynamic light scattering (DLS), while both their morphology and size were evaluated by transmission electron microscopy (TEM) using a 1% uranyl acetate solution for negative staining. The average size of LNPs was measured using Gatan Microscopy Suite (GMS) software. Reagents: 1,2-Dioleoyl-sn-glycero-3-phosphoethanolamine (DOPE), 1,2-distearoyl-sn-glycero-3-phosphoethanolamine-N-[carboxy(polyethylene glycol)-1000] (DSPE-PEG1000), and 1,2-distearoyl-sn-glycero-3-phosphoethanolamine-N-[PDP (polyethylene glycol)-2000] (DSPE-PEG2000-PDP) were purchased from Avanti Polar Lipids (Alabaster, AL, USA). Boc-Arg(Pbf)-OH and cholesterol were purchased from Sigma Aldrich (St. Louis, MO, USA). CpG oligodeoxynucleotide (CpG ODN; 5'-TCC ATG ACG TTC CTG ACG TT-3')

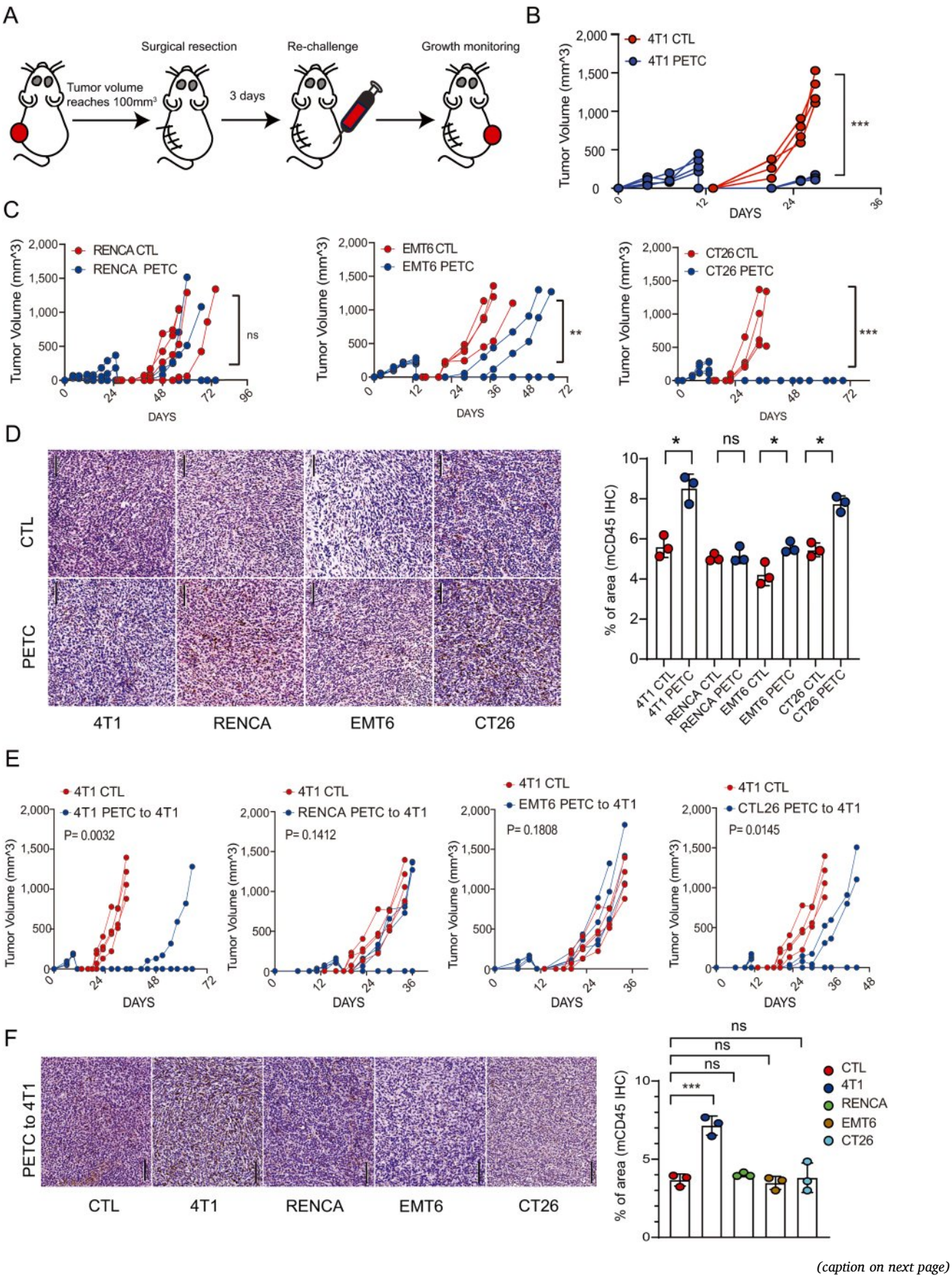

(caption on next page)

Fig. 1. Increased antitumor response of mice pre-exposed to 4T1 cells. (A) Experimental schematic for the PETC syngeneic mouse model. BALB/c mice were implanted with 4T1, RENCA, EMT6, or CT26 cancer cells in the left fat pad. Once the tumor volume reached 100 mm3, the tumor was removed surgically, followed by transplantation of the same cancer cells or 4T1 cells into the opposite fat pad. The volumes of 4T1 and RENCA (B), EMT6, and CT26 (C) tumors were monitored over a period. Four animals were included in each group. Significance was assessed using a two-way ANOVA with Bonferroni correction. $^{**}p < 0.01$, $^{***}p < 0.001$, and ns; not significant. (D) Representative immunohistochemical (IHC) images and quantification of CD45-positive cells in PETC tumors. The scale bar represents 200 μm. Each data point corresponds to an individual sample, with the error bar indicating the standard error of the mean (SEM). PETC tumors were collected from 3 mice (n=3). For each tumor, five representative imaging areas were selected, and the average intensity value from these areas was used for quantification. The growth (E) of 4T1 tumors and f CD45-positive IHC staining in mice pre-exposed to 4T1, RENCA, EMT6, and CT26 cells. Each group consisted of four animals. Significance was evaluated with two-way ANOVA with Bonferroni correction and the Mann–Whitney test. P denotes the p value. $^{***}p < 0.001$, and ns indicates not significant. The scale bar was set at 200 μm. Each data point represents an individual sample, with the error bar depicting the standard error of the mean (SEM). Three PETC tumors were collected from three mice (n=3), and for each sample, quantification was performed by averaging values from five selected imaging areas.

modified with a phosphorothioate backbone was synthesized by Genotech (Daejeon, Korea) and Bioneer (Daejeon, Korea). All unmodified peptides used in this study were synthesized by AnyGen (Gwangju, Korea).

Prior exposure to tumor cell (PETC) syngeneic mouse model

The left mammary fat pad was inoculated with 1×10^5 cells of the 4T1 and EMT6 syngeneic carcinoma cell lines, and subcutaneous inoculation was performed with 1×10^5 cells of the CT26 and RENCA cell lines. When the tumor reached 100 mm^3, it was surgically removed, and a second cell line was injected with the same quantity of cells on the opposite side.

TdL-treated syngeneic mouse model

In a prophylactic setting, 4T1 TdL was intradermally administered three times at one-week intervals, and three days after the final administration, 1×10^5 4T1 cells were injected into the left mammary fat pad per mouse. In a therapeutic setting, when 4T1 cells reached a volume of 100 mm^3, A fixed number of 4T1 TdL was administered five times at four-day intervals. The dosing schedule was based on prior pilot experiments that assessed antitumor efficacy and immune activation, and was optimized to balance therapeutic benefit with treatment tolerability.

Experimental lung metastasis mouse model

Following the protocol for the 4T1 TdL-treated syngeneic mouse model, the 4T1 cell line was injected through the tail vein, and after one month, the lungs were harvested and stained in Bouin's solution (#BOU-OT-100; BiOGNOST) for 7 hours.

CD3 and CD20 depletion mouse model

To neutralize CD3 T cells, mice were intravenously injected with either 100 μg of an anti-CD3 antibody F(ab')2 #BE0001-1FAB; Bio X cell) or 100 μg of isotype-matched hamster immunoglobulin G F(ab')2 (control IgG) (#BE0091-FAB; Bio X cell) for five consecutive days. Subsequently, peripheral blood lymphocytes (PBLs) were collected and analyzed by FACS for confirmation (Fig. S6A). Additionally, to prevent CD3 recovery induced by TdL treatment, supplementary injections were administered at one-week intervals until the mice were sacrificed. To neutralize CD20, the same protocol was followed with an in vivo antibody (#BP0356; Bio X cell and #BE0366; Bio X cell).

Combination therapy mouse model with 4T1 TdL and an anti-PDL1 antibody

Following the protocol for the 4T1 TdL-treated syngeneic mouse model in a therapeutic setting, 100 μg of anti-mouse PD-L1 (B7-H1) (#BP0101; Bio X cell) or a rat IgG2b isotype control (#BP0090; Bio X cell) was administered five times on the day following the administration of 4T1 TdL.

PEP-LNP-treated syngeneic mouse model

In a prophylactic setting, 4T1 neoantigen peptide-loaded LNPs and no peptide-loaded LNPs (control) were injected into the footpad; administration occurred three times at four-day intervals. Two weeks after the final treatment, 4T1 cells were injected into the mammary fat pad. In a therapeutic setting, once a 4T1 tumor with a volume of 100 mm^3 had formed, LNPs were injected at four-day intervals until the conclusion of the study.

Bone marrow-derived dendritic cell (BMDC) culture

BMDCs were isolated from BALB/c femurs and obtained using Pan DC MicroBeads (#130-092-465; Miltenyi Biotec, Bergisch Gladbach, Germany). The cells were suspended in RPMI-1640 medium supplemented with 10% FBS, 2-mercaptoethanol (Merck) and nonessential amino acids (Thermo Fisher Scientific, Waltham, Massachusetts, USA) and seeded in 6-well plates at a density of 1×10^6 cells/mL/well. GM-CSF (#130-095-746; Miltenyi Biotec) and IL-4 (#130-097-757; Miltenyi Biotec) were subsequently added to the medium, reaching final concentrations of 20 ng/mL each. The cells were cultured at 37°C in a 5% CO2 incubator. The culture medium was half-replaced with fresh medium at 3-day intervals, and unattached cells were transferred to new plates. On day 11, the attached cells were collected, and CD11C+ DCs were confirmed via FACS.

Pulsed BMDCs and coculture with T cells

Harvested BMDCs were seeded in 6-well plates at a density of 1×10^6 cells/mL/well, suspended with TdL or LNP antigens in medium, and incubated for 24 hours. After confirming the presence of antigen-presenting DCs (APCs) via FACS, pulsed DCs (2×10^4 cells/well) were seeded in a 96-well cell plate and incubated overnight. T cells (2×10^5 cells/well) that had been separated using CD4 (TIL) microbeads (#130-116-475; Miltenyi Biotec) and CD8 (TIL) microbeads (#130-116-478; Miltenyi Biotec) were subsequently added, and the cells were harvested 24 hours later.

Peptide-loaded LNP activity analysis

The spleens of the mice that received three injections of LNPs were harvested and dissociated into single cells, and T cells were separated using CD3ε MicroBeads (#130-094-973; Miltenyi Biotec). The secreted cytokines were subsequently measured via ELISpot following the previously described protocol of pulsing BMDCs and coculturing them with T cells.

Immunohistochemistry (IHC)

Fresh tumor tissues were collected and subsequently fixed in 4% formalin. Following fixation, the tissues were embedded in paraffin and sectioned at a thickness of 4 μm. The tissue sections were deparaffinized with xylene and rehydrated through a series of alcohol solutions. Antigen retrieval was accomplished via the use of a solution (Vector Laboratories, Inc., Burlingame, USA). To inhibit endogenous peroxidase activity, the sections were treated with 3% hydrogen peroxide and subsequently blocked with normal goat serum (ImmunoBioScience

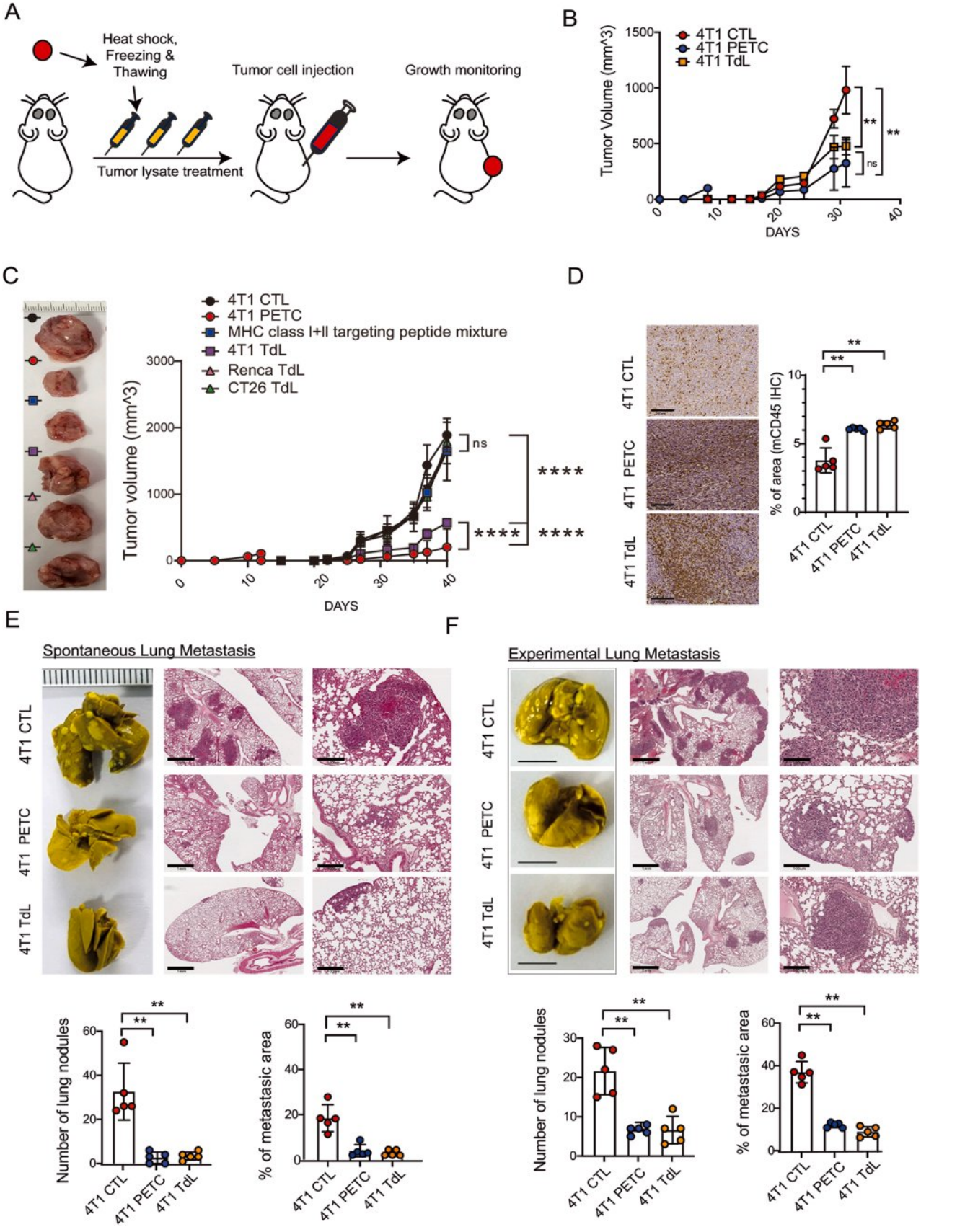

(caption on next page)

Fig. 2. Increased antitumor and anti-lung metastasis effects observed in mice pre-exposed to 4T1 cells and treated with 4T1 TdL. (A) Schematic illustration of TdL-treated mice in vivo. BALB/c mice were injected with 4T1 TdL, which was created by 41T tumor heat shock at 42°C followed by five freeze–thaw cycles. Comparison of tumor growth between CTL (untreated, n=5), 4T1 PETC (n=5), and 4T1 TdL (n=5) (B) and other treatments for 4T1 tumors, including the MHC class I+II targeting peptide mixture (n=5), Renca TdL (n=5), and CT26 TdL (n=5) groups (C). Significance was evaluated utilizing a two-way ANOVA with Tukey's HSD test. $^{**}p < 0.01$, $^{****}p < 0.0001$, and ns, not significant. (D) Images and quantification of CD45-positive cell staining in tumors. Spontaneous lung (E) metastases from untreated, 4T1 PETC-, and 4T1 TdL-treated mice were stained with hematoxylin and eosin (H&E), and experimental lung metastases are shown (F). Scale bar, 200 μm. Each data point represents an individual sample, with the error bar indicating the standard error of the mean (SEM). Significance was determined using the Mann–Whitney test. $^{**}p < 0.01$.

Corp., Mukilteo, USA). The sections were incubated at 4°C overnight with a primary antibody, i.e., anti-mCD45 (R&D, Minnesota, USA), which was diluted 1:2,000. The sections were then incubated with a secondary anti-rabbit/mouse antibody, followed by incubation in a peroxidase solution. Finally, the sections were developed using a solution from the IHC polymer detection kit HRP/DAB (Agilent, Santa Clara, USA) and counterstained with hematoxylin. Image capture was carried out using ZEN Blue 3.3 microscopy software under an optical microscope (NIKON, Tokyo, Japan). The positive signal in the IHC images was quantified using the ImageJ Immunohistochemistry (IHC) Image Analysis Toolbox.

Hematoxylin and eosin (H&E) staining

Paraffin-embedded lung tissue samples were cleared with xylene and hydrated with serial dilutions of ethanol. The samples were then sequentially stained in hematoxylin solution (#1.05175; Merck) and eosin Y solution (#1.09844; Merck).

Flow cytometry (FACS) for intracellular (cytoplasmic) and surface staining

A single-cell suspension was prepared and stained with appropriate fluorescent dye-conjugated antibodies in 5% bovine serum albumin-phosphate-buffered saline buffer (5% BSA in PBS) for 30 minutes at 4°C. For the staining of intracellular cytokines and cytoplasmic proteins, the cells were fixed with IC Fixation Buffer (#00–8222–49; Thermo Fisher Scientific) for 20–60 minutes at room temperature in the dark. Subsequently, the cells were incubated in permeabilization buffer (#00-8333-56; Thermo Fisher Scientific), followed by centrifugation at 400-600 × g for 5 minutes at room temperature. Finally, the data were acquired using a BD flow cytometer and analyzed with BD FACSDiva™ software, version 6.1.3. All information regarding the fluorescent dyes and antibodies used in the FACS analysis is described in Fig. S Table 3.

Enzyme-linked immunospot (ELISpot) assays

ELISpot assays were performed using TNF-α (#3511-4APW-2; Mabtech, Kirtlington, UK) and IFN-γ ELISpot PLUS ALP (#3321-4APT-2; Mabtech) kits following the manufacturer's protocol with stimulated T cells (2.0×10^5 cells/well). The spots were counted using an automated spot counter (ImmunoSpot® CTL S6 Micro Analyzer; Cellular Technology Limited) within 24 h, and the spot counts were further analyzed as the number of spot-forming units (SFUs) per well. The Immunospot settings employed included a sensitivity of 145 or 187, background balance of 10, spot separation of 1–3, and spot size ranging from a minimum of 0.0015 to a maximum of 9.6296 or 9.6466 mm^2. These parameters were fine-tuned for optimal resolution and accurate spot enumeration. The raw data included images for each well, facilitating visual quality inspection, in addition to the corresponding spot-forming unit (SFU) counts per well.

Single-cell sequencing analysis

The single-cell RNA sequencing data were mapped to the mm10 mouse reference genome using CellRanger (10X Genomics) version 6.0.0. The aligned data were further clustered using the Seurat (v4.1.0) package in R. Cells with < 200 or > 2,500 RNA features and > 5% mitochondrial sequences were filtered out to ensure high quality. The data were then processed with the suggested pipeline, including log normalization, data scaling, principal component calculation, UMAP calculation, defining neighbors with 1:20 dimensions, and finding clusters with a resolution of 0.9. For TdL, three datasets were incorporated, and batch correction was performed with Harmony. The cells were first annotated using the 'ImmGenData' reference in the Celldex package and the 'PBMC' reference in the Azimuth package and were compared and evaluated manually by examining marker gene expression for each cell type. Differential gene expression across different conditions was calculated with the 'FindMarkers' function in Seurat. Genes with an adjusted p value of 0.05 were considered significant. The percentages of the different cell populations were plotted with ggplot2. Gene expression across different cell types was first calculated with the 'AverageExpression' function in Seurat and then plotted with the pheatmap package in R.

RNA sequencing and gene ontology (GO) analysis

Trimmomatic (v.0.39) was used to remove adapter sequences. We then aligned the remaining reads to the GRCm39 (mm10) construct and assigned genes on the basis of the gene structure information from GENCODE (Mus_musculus.GRCm39.104.gtf) using STAR (v.2.7.10a) with 2-pass mapping. Gene expression values were quantified using RSEM (v1.3.1). Differential gene expression was assessed with DEseq (v1.30.1). To identify significantly enriched pathways through the Kyoto Encyclopedia of Genes and Genomes (KEGG) [20], we utilized the DAVID (Database for Annotation, Visualization, and Integrated Discovery, https://david.ncifcrf.gov/) database. We considered a P value less than 0.05 to indicate statistical significance.

Statistical analysis

Statistical analysis for this study was performed with GraphPad Prism 8.2 software (GraphPad Software, Inc., San Diego, CA). The results are presented as means ± standard errors (SEMs). To assess statistical significance, the t test was employed to compare two populations, and ANOVA was used to compare more than two populations under the assumption of a normal distribution. In cases of a nonnormal distribution, the Mann–Whitney U test was applied to compare two populations, and the Kruskal–Wallis H test was used to compare more than two populations. A p value of less than 0.05 was considered statistically significant, denoted as * $p < 0.05$, ** $p < 0.01$, *** $p < 0.001$, and **** $p < 0.001$.

Data availability

The experimental data produced in this study are included in the main text, figures, or the supplementary information/Source Data File. This source data is provided with the paper.

Results

Mice with prior exposure tumor cell (PETC) develop antitumor effects for subsequent tumor challenge

We exposed BALB/c mice to syngeneic 4T1 murine mammary

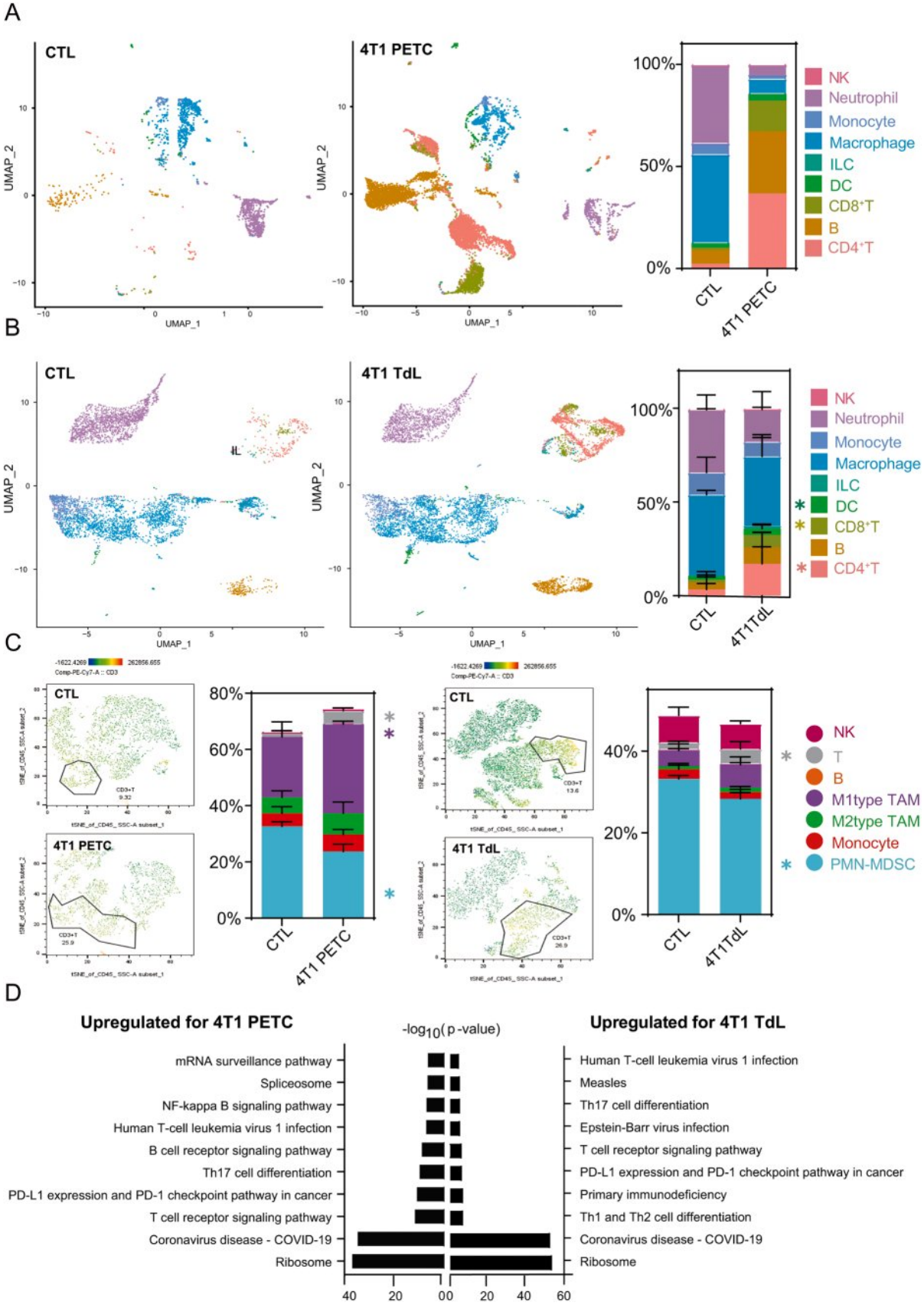

(caption on next page)

Fig. 3. PETC and TdL modify the identification of immune cell types within tumors. Uniform manifold approximation and projection (UMAP) plot depicting the characterized cell clusters derived from tumors in mice previously exposed to 4T1 cells (A) and treated with 4T1 TdL (B), including natural killer (NK) cells, neutrophils, monocytes, macrophages, innate lymphoid cells (ILCs), dendritic cells (DCs), CD8+ T cells, B cells, and CD4+ T cells. Each sample was analyzed for CTL (n=1) and 4T1 PETC (n=1) – total number of analyzed cells: 1159 (CTL) and 3360 (4T1 PETC), and for CTL (n=3) and 4T1 TdL (n=3) – total number of analyzed cells: 3820 (CTL) and 5253 (4T1 TdL), with error bars indicating the standard error of the mean (SEM). Significance was determined via the Mann–Whitney test, with *$p < 0.05$. (C)The flow cytometry analysis of tumors included a representative t-SNE visualization of the T cell population and bar graph of all immune cell subsets, such as NK cells, T cells, B cells, M1 tumor-associated macrophages (M1 TAMs), M2 tumor-associated macrophages (M2 TAMs), monocytes, and polymorphonuclear myeloid-derived suppressor cells (PMN-MDSCs). Each sample was subjected to analysis for CTL (n=3) and 4T1 PETC (n=3), as well as for CTL (n=3) and 4T1 TdL (n=3), with error bars indicating the standard error of the mean (SEM). The data were used to quantify 100% of the immune cells, and the Mann–Whitney test was used to determine significance, with *$p < 0.05$. (D) KEGG pathway analysis of the top 10 differentially expressed genes (DEGs) for the immune cell populations identified via single-cell sequencing of tumors from mice pre-exposed to 4T1 cells or treated with 4T1 TdL.

carcinoma cells by briefly growing the tumors *in vivo* and removing them through surgical resection (Fig. 1A). Upon rechallenging these mice with 4T1 cells, we observed significantly delayed tumor growth compared with that observed for unexposed mice (Fig. 1B). We then investigated whether other syngeneic cell lines would induce similar antitumor effects in mice following brief exposure. Fig. 1C shows that different cancer cell lines produced varying degrees of antitumor effects, with CT26 cells (colonic carcinoma cell line) and RENCA cells (kidney carcinoma cell line) showing the greatest and lowest effects, respectively. 4T1 and CT26 tumors in the mice pre-exposed to tumor cells presented significantly increased numbers of infiltrating immune cells in the TME (Fig. 1D).

To determine whether the observed antitumor effect of prior exposure was cell line-specific for 4T1 cells, we exposed mice to various cell lines and subsequently injected them with 4T1 cells. Prior exposure to 4T1 cells significantly reduced subsequent tumor growth, while exposure to RENCA (kidney carcinoma cell line) or EMT6 cells (mammary carcinoma cell line) had no such effect (Fig. 1E). Prior exposure to CT26 cells did not reduce tumor growth in two out of three mice. An increase in the number of immune cells in the TME of 4T1 tumors was observed only in the mice that were pre-exposed to 4T1 cells (Fig. 1F). These data indicate that PETC can induce antitumor effects and immune microenvironment remodeling in a subset of cancer cell lines, including 4T1 mammary carcinoma cells.

Tumor cell-derived lysates (TdLs) effectively inhibit tumor growth and metastasis

Next, we prepared TdLs through repeated cycles of freezing and thawing and administered the TdLs prior to tumor cell injection to investigate whether the TdLs generated a similar antitumor effect in 4T1 mammary carcinoma models (Fig. 2A). As shown in Fig. 2B, 4T1 TdL elicited an antitumor response similar to that of prior exposure to 4T1 cells. The antitumor effect of TdLs was not affected by the use of poly I:C (Fig. S1). TdLs derived from other cell lines, such as RENCA or CT26 cells, did not have inhibitory effects on 4T1 tumor growth (Fig. 2C).

Like prior exposure to 4T1 cells, the 4T1 TdL induced an increase in immune cell infiltration in the TME (Fig. 2D). Prior exposure to 4T1 cells or 4T1 TdL administration resulted in a significant reduction in spontaneous lung metastasis in the 4T1 orthotopic injection model (Fig. 2E). Additionally, both PETC and TdL reduced experimental lung metastasis in the 4T1 tail-vein injection model (Fig. 2F). These data indicate that TdLs can induce antitumor immune effects that inhibit tumor growth and metastasis in a 4T1 mammary carcinoma model.

PETC- or TdL-induced tumor immune microenvironment (TIME) remodeling

To investigate the effects of PETC and TdLs on the TIME, we conducted single-cell sequencing of tumor tissues. Prior exposure to 4T1 cells resulted in significant remodeling of the TIME, with an increased presence of B cells, $CD4^+$ T cells, and $CD8^+$ T cells (Fig. 3A). The administration of TdLs resulted in a similar change in the TIME, with a statistically significant increase in the number of $CD4^+$ and $CD8^+$ T cells (Fig. 3B). Both PETC and TdLs led to a reduction in the number of neutrophils and monocytes. Flow cytometry analysis also revealed an increased number of T cells in the TIME of 4T1 tumors pre-exposed to tumor cells or treated with TdL (Fig. 3C and Figures S2A and B). Additionally, flow cytometry data revealed that PETC and TdLs significantly reduced the number of PMN-MDSCs in the TIME. These data indicate that the antitumor effect of the PETC or TdLs can be caused by substantial remodeling of the immune cell population in the TIME of 4T1 tumors.

Transcriptomic features of tumors pre-exposed to tumor cells or TdLs

We explored single-cell RNA sequencing data to further characterize the transcriptomic features of the TIME associated with both PETC and TdL administration. The transcriptome features of the TIME suggested substantial alterations in gene expression in immune-related pathways in both experimental groups. The commonly altered pathways included human T-cell leukemia virus 1 infection, Th17 cell differentiation, T-cell receptor signaling, PD-L1 expression and PD-1 checkpoint pathways in cancer (Fig. 3D).

Next, we investigated the TIME genes that were differentially expressed when models were pre-exposed to tumor cells or administered TdL. A total of 383 and 59 genes were significantly differentially expressed after PETC and TdL administration, respectively. There were 12 co-upregulated genes and 35 co-downregulated genes (Fig. 4A). Interestingly, when the genes were hierarchically clustered, the upregulated genes were predominantly associated with $CD4^+$ T cells, $CD8^+$ T cells, and B cells. In contrast, the majority of downregulated genes were observed in myeloid lineage cells, especially neutrophils (Fig. 4B). These data indicate that PETC and TdL administration resulted in functional remodeling in the TIME, in addition to the abovementioned quantitative shift.

Among the genes showing differential expression, the *Il7r, Cd3d*, and *Lef1* genes are associated with adaptive memory T cells [21–23]. We observed a significant increase in the expression of the Il7r, Cd3d, and Lef1 genes in the T cell subpopulation (Fig. 4B and Figure S3). Additionally, FACS analysis of the TIME revealed increased numbers of effector memory $CD8^+$ T cells and central memory $CD4^+$ T cells when the mice were treated with TdLs (Fig.s 4C and S4). Notably, the CD4/CD8 ratio in the TME was significantly increased in the 4T1 TdL group. An increase in effector memory $CD8^+$ T cells after TdL treatment was also observed in the blood (Figures S5A and S5B). To explore changes in the nonimmune compartment in detail, we analyzed the results from both bulk RNA sequencing and single-cell sequencing (Fig. 4D). The findings revealed a notable increase in the *Pdgfα* and *Tmem132a* genes, particularly in the cancer epithelial cells of TdL-treated mice. *Pdgfa* [24] is associated with tumor-promoting processes such as stromal remodeling and angiogenesis, while *Tmem132a* [25] has been linked to epithelial cell adhesion and signaling. The upregulation of these genes suggests that TdL treatment may enhance tumor-stromal interactions and modulate epithelial cell states. These data indicate that PETC or TdL treatment induces dynamic transitions in the transcriptomic phenotypes of diverse

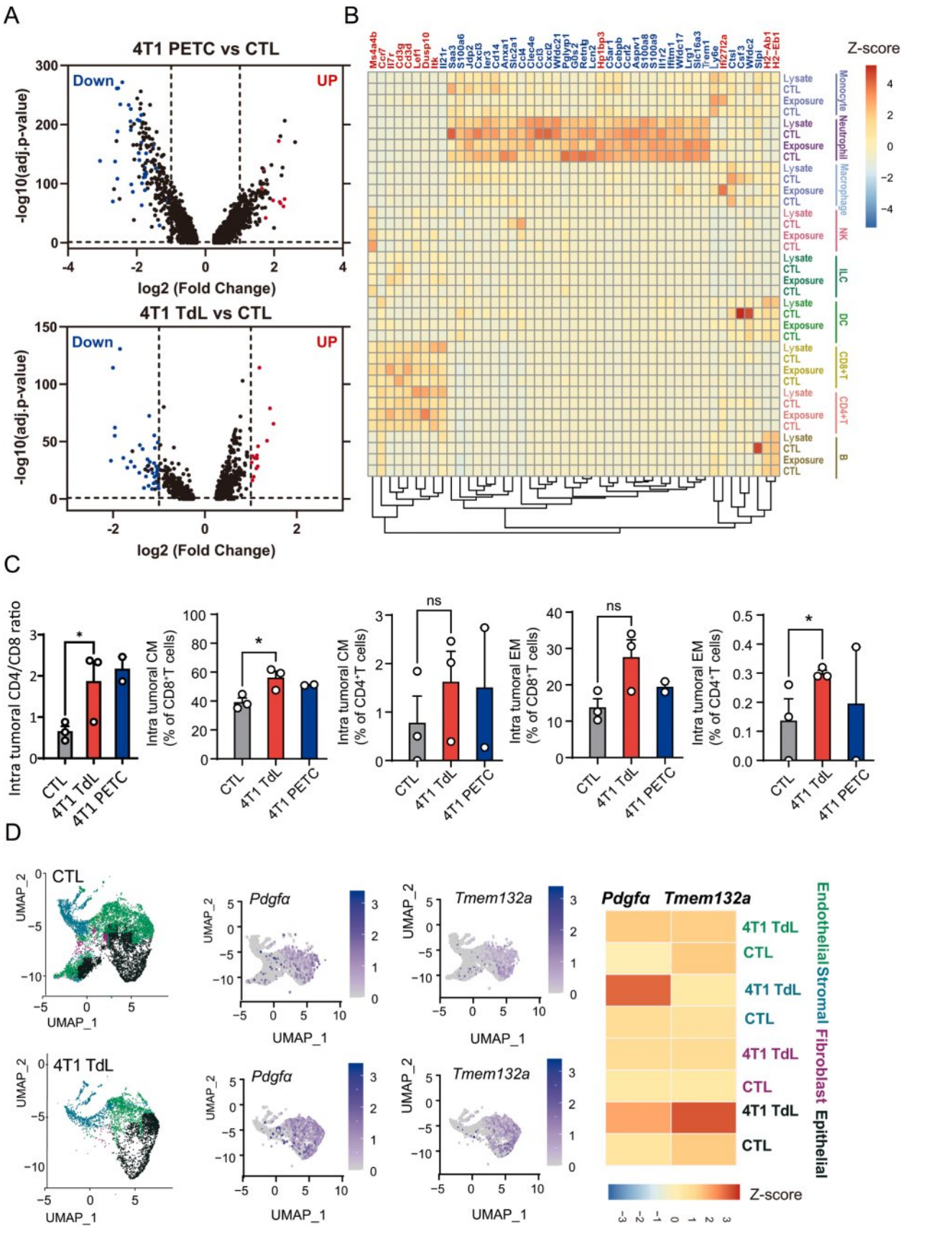

(caption on next page)

Fig. 4. Transcriptomic characteristics of cell types altered by pre-exposure to 4T1 cells or treatment with 4T1 TdL. (A) Volcano plot displaying protein abundance comparisons for tumors from mice pre-exposed to 4T1 cells (top) and or treated with 4T1 TdL (bottom), which revealed significant differences (log2-fold change greater than 1, -log10 adjusted p value greater than 0). The same gene list is represented with upregulated genes shown as red dots and downregulated genes as blue dots. (B) Heatmap illustrating the quantity of all significantly differentially abundant genes across immune cell types for tumors from mice pre-exposed to 4T1 cells or treated with 4T1 TdL, with a color legend indicating each cell cluster. The expression values were normalized by row. Red indicates upregulated genes, and blue indicates downregulated genes. (C) FACS analysis was performed to assess the frequency of central memory ($CD62L^+CD44^+$) and effector memory ($CD62L^-CD44^+$) cells within the $CD4^+$ or $CD8^+$ T cell populations obtained from tumors (CTL; n=3, 4T1 TdL; n=3, 4T1 PETC; n=2). The data were normalized to the total number of $CD4^+$ or $CD8^+$ T cells (set as 100%), and statistical significance was evaluated using the Mann–Whitney test (*$p < 0.05$; ns = not significant). (D) In this dataset, the genes commonly upregulated in tumors treated with 4T1 TdL, as derived from RNA sequencing (RNA-seq) and nonimmune clusters identified via single-cell sequencing, are Pdgfα and Tmem132a. The representative UMAP illustrates Pdgfα and Tmem132a (left), and the heatmap shows z scores of single-cell sequencing transcripts, which are divided into four clusters, namely, endothelial, stromal, fibroblast, and epithelial cells (total number of analyzed cells: CTL; 2960 and 4T1 TdL; 742) in the right panel.

cell populations in tumor tissues.

PETC and TdLs modulate the T cell antitumor response

To investigate the functional roles of T cells during the TdL-induced antitumor response, we depleted T cells with an anti-CD3 monoclonal antibody (α-CD3 mAB) before 4T1 TdL injection (Fig. 5A). In the T cell-depleted mice, the injection of TdL failed to induce significant tumor inhibition (Fig. 5B). Interestingly, the depletion of B cells with an anti-CD20 monoclonal antibody (α-CD20 mAB) resulted in the opposite response in mice. In the α-CD20 mAb-treated mice, the inhibition of tumor growth was greater than that in the isotype-treated mice (Figure S6). These observations indicate that while T cells are critical in the PETC- and TdL-induced antitumor response, additional studies are essential to elucidate the complex roles of B cells.

To demonstrate the antitumor effect of T cells, dendritic cells were isolated from mouse bone marrow and pulsed with TdL *ex vivo*. Compared with control dendritic cells, TdL-pulsed dendritic cells presented an enhanced antigen-presenting phenotype (Fig.s 5C and S7). Additionally, we isolated T cells from the TIME of experimental mouse tumors and tested T cell cytotoxicity *ex vivo* after they were cocultured with dendritic cells. TIME-generated T cells isolated from mice subjected to PETC or TdL treatment presented significantly increased cytotoxicity against tumor cells (Fig. 5D).

Enzyme-linked immunospot (ELISpot) experiments revealed that PETC and TdL treatment significantly increased the secretion of TNF-α from $CD4^+$ T cells and the secretion of IFN-γ from $CD8^+$ T cells (Fig. 5E). Additionally, intratumoral FACS analysis revealed an increase in the number of Granzyme B-expressing $CD8^+$ T cells and perforin-expressing $CD4^+$ T cells in PETC tumors (Fig. 5F) and in the number of CRTAM-expressing $CD4^+$ and $CD8^+$ T cells in TdL-treated tumors (Fig.s 5G and S8). Collectively, these findings indicate that the antitumor immunity induced by PETC and TdLs is regulated by the increased antitumor functionality of T cells in the TIME.

TdLs effectively reduce tumor growth and metastasis in mice with pre-existing tumors

While the above data demonstrate that TdL treatment prior to tumor implantation can inhibit subsequent tumor growth and metastasis, the translational implications of a prophylactic TdL treatment strategy are severely limited by the fact that all human solid tumors have unique and unpredictable mutational profiles. To address this issue, we tested whether 4T1 TdL treatment can induce antitumor effects in mice that harbor preexisting 4T1 tumors by administering TdL after the tumors reached a volume of 100 mm^3 (therapeutic TdL, Fig. 6A). Therapeutic TdLs significantly reduced the growth of 4T1 tumors (Fig.s 6A and S9) and increased the number of immune cells in the TIME (Fig. 6C). Additionally, therapeutic TdL treatment significantly reduced the number of lung metastases in both spontaneous and experimental 4T1 lung metastasis models (Fig.s 6D and E).

Therapeutic TdL treatment induced TIME remodeling by increasing the presence of T cells and B cells, similar to what was observed with PETC or prophylactic TdL treatment (Fig.s 6F and S10). Furthermore, the T cells isolated from the TIME of the tumors treated with TdL therapeutically significantly increased the *ex vivo* antitumor capacity (Fig. 6G). Intratumoral FACS analysis revealed that the number of CRTAM-expressing T cells increased with therapeutic TdL treatment (Fig.s 6H and S11), and the ELISPOT data revealed that the secretion of TNF-α and IFN-γ from T cells increased (Fig. 6I). Additionally, therapeutic TdL treatment significantly reduced the number of exhausted T cells in the draining lymph nodes, as determined by the number of $TIGIT^+$ and $PD1^+$ $CD4^+$ T cells calculated via intratumoral FACS analysis (Figure S12).

The addition of therapeutic TdL treatment significantly enhances the efficacy of anti-PD-L1 monoclonal antibodies in 4T1 mouse mammary carcinoma models

As shown in Fig. 3D, prior exposure to 4T1 cells and 4T1 TdL administration resulted in the significant upregulation of the genes involved in the PD-L1 pathway. On the basis of these findings, we hypothesized that therapeutic TdL administration may increase the efficacy of α-PD-L1 mAbs toward syngeneic 4T1 tumors. To test this hypothesis, we administered therapeutic TdL in combination with an α-PD-L1 mAb when the 4T1 tumors reached a volume of 100 mm^3 (Fig. 7A). The α-PD-L1 mAb alone minimally inhibited tumor growth, but when combined with therapeutic TdL, the α-PD-L1 mAb highly effectively suppressed tumor growth in a 4T1 mammary carcinoma model (Fig. 7B).

To investigate the potential TIME remodeling associated with TdL in combination with an α-PD-L1 mAB, we performed single-cell RNA sequencing using tumor tissues treated with an α-PD-L1 mAB with or without TdL. As shown in Fig. 7C, we observed increased numbers of macrophages, dendritic cells, and $CD4^+$ T cells in tumors treated with TdL plus an α-PD-L1 mAb. Additionally, we observed a set of DEGs in tumors treated with TdL plus an α-PD-L1 mAB (Figure S13). Among the DEGs, genes associated with increased efficacy of immune checkpoint antibodies, such as Rgs1, Xist, and Ccl7 [26–29], were upregulated in the macrophages and monocytes of TdL-treated tumors. Additionally, genes involved in resistance to immune checkpoint antibodies, including Lrg1, S100a8, and S100a9 [30,31], were downregulated in the neutrophil population (Fig. 7D). These data indicate that TdL administration in combination with an α-PD-L1 mAb can substantially increase antitumor efficacy by remodeling the TIME.

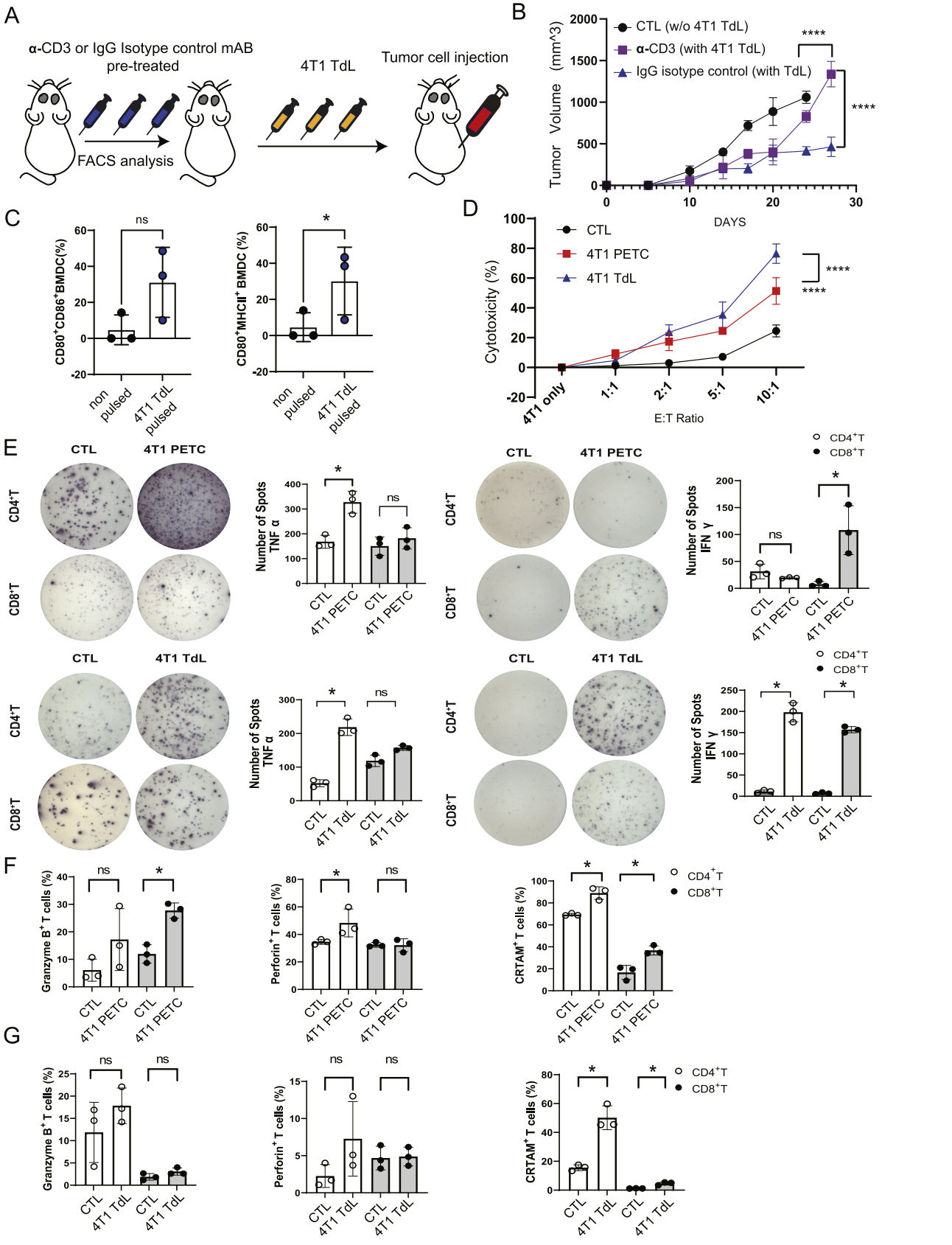

(caption on next page)

Fig. 5. PETC and TdL play key roles in regulating the antitumor response of T cells. (A) Schematic illustration of the CD3+ T-cell-depleted or IgG isotype control mouse model used to identify the effects of treatment with 4T1 TdL. (B) Five mice in each group, treated with either anti-CD3 or an IgG isotype control, received a total of three treatments with 4T1 TdL or control formulations, and the tumor volumes were subsequently measured. Significance was evaluated via two-way ANOVA, with ****$p < 0.0001$. (C) FACS analysis was performed to evaluate the presence of CD80+CD86+ (left) or CD80+MHCII+ (right) BMDCs after 4T1 TdL pulsing. The Mann–Whitney test was conducted, with *$p < 0.05$; ns indicates not significant, with error bars representing the standard error of the mean (SEM). We evaluated the functionality and cytotoxicity of T cells isolated from mice pre-exposed to 4T1 cells or treated with 4T1 TdL (n=3). To confirm the antigen-specific immune responses of all the T cells isolated from the immunized mice, we cocultured the T cells with DCs pulsed with 4T1 TdL in vitro. (D) Cytotoxicity was evaluated via the LDH assay, considering the numerical changes in the ratio of effector (T) cells isolated from the spleen to target (4T1) cells (n=3). Two-way ANOVA with Tukey's HSD was performed, and the results were statistically significant at ****$p < 0.0001$. TNF-α and IFN-γ secretion from CD4+ and CD8+ T cells isolated from tumors (n=3) was measured via ELISpot assays. ELISpot assays were used to measure the levels of TNF-α and IFN-γ secretion (E), while intracellular FACS analysis was used to assess the representative expression (Granzyme B, perforin, and CRTAM) in cytotoxic T lymphocytes (CTLs) from CD4+ and CD8+ T cells isolated from tumors from mice pre-exposed to 4T1 cells (F) and treated with 4T1 TdL (G) (n=3). The Mann–Whitney test was performed; statistical significance is denoted by *$p < 0.05$, and "ns" indicates not significant. Error bars represent the standard error of the mean (SEM).

Neoantigen peptide-loaded lipid nanoparticles can induce a tumor-specific antitumor effect in a 4T1 mammary carcinoma model

To identify potential neoantigens in 4T1 mammary carcinoma cells, we generated exome and transcriptome sequencing data from control and PETC tumors and processed the sequencing data via the DeepNeo platform (Table S1). On the basis of the neoantigen selection criteria described in the Methods section, we identified and synthesized three T cell-reactive neoantigen peptides and loaded them on LNPs, as shown in Fig. 8A (Table S2). In addition, we identified Dtx2, Gk, and H2afy as genes encoding peptides with high predicted binding affinity to both MHC class I and II molecules, indicating their potential to stimulate both $CD8^+$ cytotoxic and $CD4^+$ helper T cell responses. These dual-binding neoepitopes may enhance the overall immunogenicity of the tumor microenvironment by engaging multiple arms of the adaptive immune system. The administration of neoantigen peptide-loaded LNPs significantly increased the number of dendritic cells with an antigen-presenting phenotype to a degree similar to that observed for the TdL treatment (Fig.s 8B and C). As expected, the secretion of TNFα and IFNɣ from T cells from mice treated with neoantigen peptide-loaded LNPs significantly increased when the cells were cocultured with BMDCs pulsed with LNPs (Fig. 8D). Importantly, the increased secretion of TNFα and IFNɣ from T cells from mice treated with neoantigen peptide-loaded LNPs was also observed when the cells were cocultured with BMDCs pulsed with TdLs (Fig. 8D). These data suggest that neoantigen peptide-loaded LNPs can induce neoantigen-specific immunogenicity in mice.

Next, we tested the *in vivo* antitumor effect of neoantigen peptide-loaded LNPs in mice harboring 4T1 tumors. As shown in Fig. 8E, LNPs loaded with neoantigen peptides targeting T cells had significant antitumor effects when they were administered prior to or after 4T1 tumor injection. Single-cell sequencing data also revealed an increased number of T cells in the TIME with neoantigen peptide-loaded LNPs (Fig. 8F). Finally, neoantigen peptide-loaded LNPs significantly reduced the number of lung metastases in the 4T1 mammary carcinoma model *in vivo* (Fig. 8G).

Discussion

Triple-negative breast cancer (TNBC) represents a molecularly diverse subset of breast carcinomas characterized clinicopathologically by the absence of estrogen and progesterone receptors as well as the absence of human epidermal growth factor-2 (HER2) overexpression (REF). This aggressive malignancy constitutes approximately 15% of all breast cancers and carries a significant risk of distant disease recurrence and mortality [32]. Given the limited treatment options and poor prognosis associated with TNBC, the aim of our study was to explore innovative neoantigen-based immunotherapeutic approaches to improve patient outcomes.

Traditionally, the systemic treatment of TNBC relies mainly on cytotoxic chemotherapy, which commonly uses anthracycline or taxanes. To identify additional effective therapeutic options, efforts have focused on understanding the role of the immune system in TNBC progression and exploiting antitumor immunity. The pivotal discovery of immune checkpoint blockade (ICB) has shown promise across different tumor types, supporting the potential for similar approaches in TNBC [33]. However, unlike other solid tumors, such as melanoma and lung cancer, breast cancers generally exhibit limited lymphocyte infiltration and lower mutational burdens (TMB), suggesting reduced immunogenicity and leading to the perception of breast tumors as "immune cold" [34,35]. Therefore, enhancing neoantigen presentation and immune priming in TNBC is critical for improving therapeutic efficacy.

Our study addressed three important issues regarding the therapeutic potential of modulating antitumor immunity and the TIME through innovative immunotherapeutic approaches targeting tumor-specific antigens in TNBC. First, we demonstrated that prior exposure to 4T1 cells, TdLs, and neoantigen peptide-loaded LNPs significantly reduced tumor growth and metastasis in a syngeneic 4T1 murine mammary carcinoma model. In addition, several peptides—such as those derived from Dtx2, Gk, and H2afy—were predicted to have high binding affinity for both MHC class I and II molecules, suggesting the potential to stimulate not only $CD8^+$ T cells but also $CD4^+$ helper T cells. This dual MHC-binding property may enhance the breadth and durability of the antitumor immune response by engaging multiple arms of the adaptive immune system and promoting effective T cell priming within the tumor microenvironment. However, one major concern raised is whether the observed immune response was predominantly neoantigen-driven or largely mediated by tumor-associated antigens (TAAs). While it is true that TdLs and PETC contain a mix of TAAs and other immunogenic components, our study provides compelling evidence that neoantigen-specific immunity plays a key role in tumor control. In the process of inducing an antigen-specific antitumor effect in the TIME, tumor cells carry abundant endogenous mutated proteins that are degraded into peptides and displayed on the tumor cell surface. These peptides prompt immune recognition as "nonself" entities [36,37]. Tumor cells present these antigenic epitopes on major histocompatibility complex (MHC) molecules, which are recognizable by T cells, making them essential for the specific identification and elimination of cancer cells [38,39]. Additionally, LNPs effectively protect 4T1 neoantigen peptides from degradation, facilitate their intracellular delivery, and enable endosomal escape, allowing the peptides to function properly within the cell. LNPs have been utilized in various cutting-edge treatments for solid cancers, including breast cancer [40]. Another innovative application involves the use of LNPs to deliver mRNAs encoding cytokines such as IL-12 and IL-27 directly into tumors to modulate the TME and enhance the antitumor immune response, showing efficacy in preclinical models [41]. Notably, we also observed a significant increase in the quantity of reactive T cells and their efficacy in eliminating 4T1 tumors in our murine breast cancer model when a diverse range of antigen-based treatments were employed. Reactive $CD8^+$ and $CD4^+$ T cells that target tumor-specific

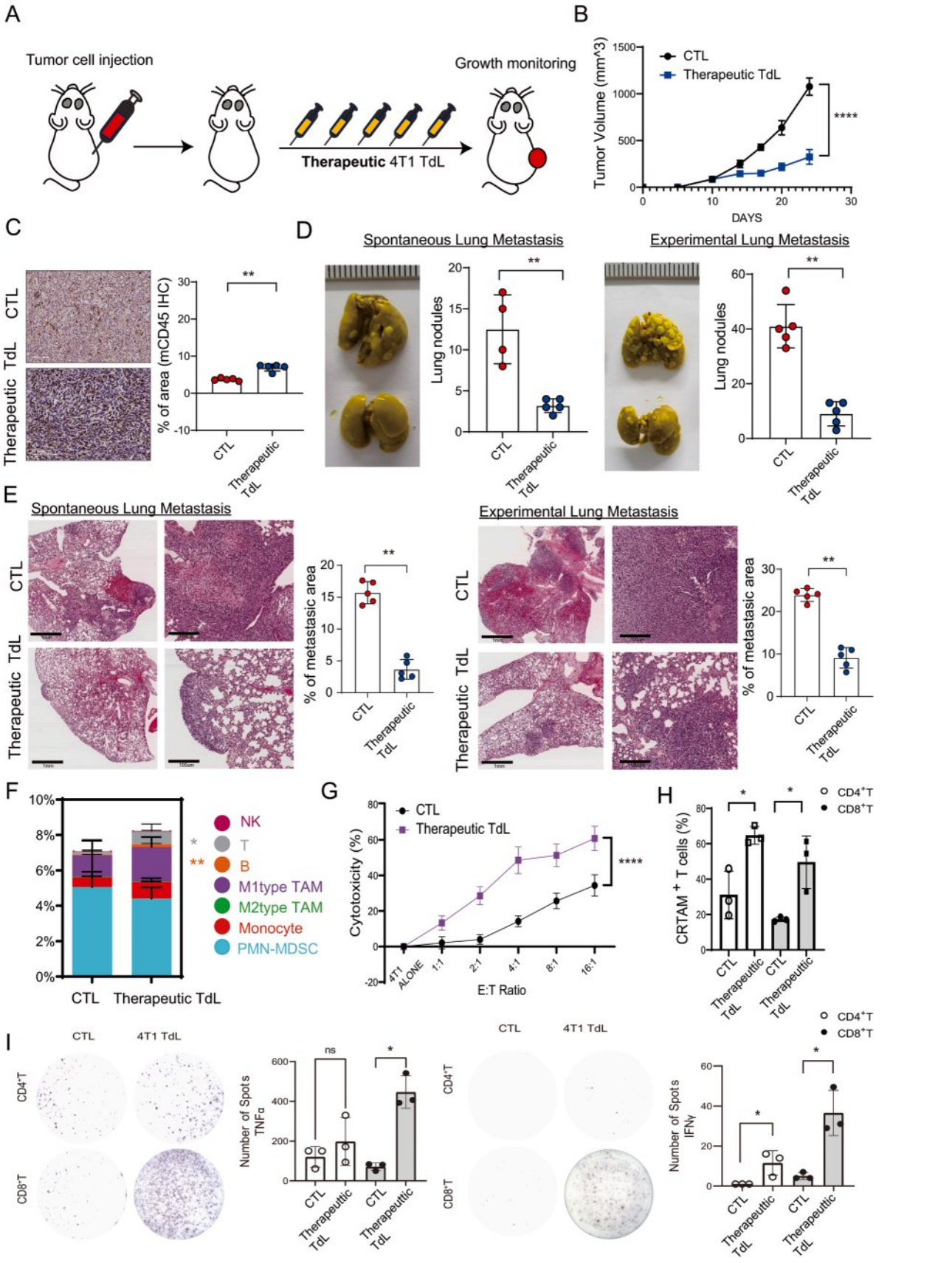

(caption on next page)

Fig. 6. Therapeutic TdL induces an effective antitumor response. (A) Diagram illustrating the therapeutic mechanism of 4T1 TdL; treatments were administered every 4 days once the tumor volume reached 100 mm3, and tumor growth was monitored (B). Two-way ANOVA with Tukey's honestly significant difference (HSD) test was performed, with ****$p < 0.0001$. (C) IHC analysis of CD45+ cell infiltration in tumors from mice treated with 4T1 TdL or control formulations. Scale bars, 100 μm. The Mann–Whitney test was performed, with **$p < 0.01$. Mice ($n = 5$) were inoculated either subcutaneous or intravenously with 4T1 tumor cells on day 0 and immunized every 7 days with 4T1 TdL or control formulations. Representative image of lung nodules (D) and microscopy image of the metastasized area (E) in lung metastasis after subcutaneous or intravenous injection of 4T1 tumor cells. Scale bar, 100 μm. Statistical significance was determined via the Mann–Whitney test; SEMs are provided, with **$p < 0.01$. (F) Immune profiling via FACS was performed for tumors from mice treated with therapeutic TdL or control formulation. The Mann–Whitney test was performed, with *$p < 0.05$ and **$p < 0.05$. To verify the 4T1 antigen-specific T cell immune response, 4T1 TdL-pulsed BMDCs cocultured with T cells were isolated from mice treated with 4T1 TdL or control formulations (n=3). Subsequently, analysis was conducted via (G) LDH assays, (H) intracellular FACS for CRTAM expression, and (I) ELISpot assays. Statistical significance of the data in panel (J) was calculated via two-way ANOVA with Bonferroni correction, that of data in panels (H) and (I) was calculated with the Mann–Whitney test; *$p < 0.05$ and ****$p < 0.0001$.

antigens have been identified in various human cancers, including melanoma [42], leukemia [43], ovarian cancer (OC) [44], and cholangiocarcinoma [45]. Prior studies, including those by Spranger et al. (J Clin Invest. 2021) and Wu et al. (J Immunother Cancer 2022), have demonstrated the efficacy of neoantigen-based cancer vaccines in TNBC models. The former showed that radiotherapy could enhance neoantigen presentation, thereby increasing CD8+ and CD4+ T cell-mediated tumor control. Similarly, the latter highlighted the potential of personalized multi-neoantigen vaccines using viral-like particles (VLPs) to elicit robust immune responses. Our findings align with these studies while also presenting a distinct approach: enhancing tumor antigen presentation through prior exposure and nanoparticle-mediated delivery of neoantigenic peptides. Importantly, we observed a significant increase in the quantity and functionality of neoantigen-reactive T cells, particularly CD8+ and CD4+ T cells, in our model. Neoantigen-specific T cell responses have been extensively characterized in human cancers, including melanoma, leukemia, and ovarian cancer, and our data suggest that TNBC can similarly generate antigen-specific cytotoxic immune responses. The efficacy of LNPs in stabilizing and delivering neoantigen peptides further supports their potential as a non-viral platform for therapeutic vaccination. Unlike whole-cell or lysate-based approaches, LNP-mediated delivery ensures targeted intracellular delivery, enhancing antigen processing and presentation via MHC class I and II molecules.

Second, genomic and transcriptomic analyses can provide insights into the inherent characteristics and external factors influencing the response of tumors to emerging immunotherapies. Studies on intratumoral lymphocyte infiltration in patients with localized breast carcinoma have produced conflicting results regarding its influence on therapeutic resistance [46]. Our study explored how genomic-scale gene expression in various immune cell types intersects with the transcriptomic profile of tumors, particularly in response to immunotherapy. Genetic markers indicative of immune responsiveness have been identified in various tumors, including colon adenocarcinomas [47,48], melanoma [49,50], and lung cancer [51]. Importantly, we previously examined the potential of gene expression features of memory T cells (*Il7r, Cd3d,* and *Lef1*) and positive responses to checkpoint blockade (*Rgs1, Xist, Ccl7* and *S100a8&9*) to predict the efficacy of neoantigen-targeting immunotherapy in breast cancer [52,53].

Multiple strategies have been developed to create cancer vaccines using tumor antigens delivered as whole cells [54], nucleic acids [54,55], peptides, or proteins [56,57]. The utilization of whole tumor cell lysates is effective for treating all cancer patients, irrespective of their HLA type. Targeting both tumor cells and the tumor stroma is proposed as an effective strategy for eliminating established tumors. Melanoma, with its high tumor mutation burden (TMB), is an excellent candidate for cancer vaccine treatment. Talimogene laherparepvec (T-VEC, tradename IMLYGIC) became the first FDA-approved oncolytic viral drug for advanced melanoma in 2015 [58]. Clinical trials are investigating autologous dendritic cells loaded with tumor lysate or peptides, which have shown significant immunogenicity and antitumor efficacy in patients with localized metastatic melanoma (NCT00107159, NCT01876212). sipuleucel-T (Provenge), a dendritic cell vaccine for metastatic castration-resistant prostate cancer (mCRPC), received FDA approval in 2010 [59]. A clinical trial demonstrated that a DNA vaccine (pTVG-HP), encoding prostate tumor antigen prostatic acid phosphatase (PAP), effectively enhanced the immune response after immunization with sipuleucel-T in mCRPC patients (NCT01706458).

Despite these advancements, there are no FDA-approved therapeutic breast cancer vaccines, and the results of clinical trials have been disappointing [60]. However, in a recent trial (NCT00880464), an irradiated GM-CSF-secreting breast cancer lysate vaccine showed coordinated immune responses with minimal toxicity in metastatic and stage II-III breast cancer patients. Although our study is preclinical, we observed an antigen-specific CTL immune response to shared antigens after preexposure to 4T1 cells and 4T1 TdL treatment, identifying key immune populations involved in antitumor activity. Analyzing gene expression among individual immune cells provides clinical insights for targeting these cells. The process of creating therapeutic treatments using tumor-derived antigens is promising, as it safely and efficiently induces an antitumor effect in breast cancer patients by using the patient's tumor to create TdL and synthetic peptide-loaded LNPs, providing autologous treatment without viral vectors. Additionally, the tumor inhibition and increased infiltration of lymphocytes observed with preexposure to CT26 cells suggest the potential development of a promising anticancer agent for other challenging solid cancers, such as colorectal cancer. Furthermore, we observed inhibited tumor growth and lung metastasis in 4T1 tumors with PETC, treated with prophylactic TdLs, and administered peptide LNPs, suggesting promising prospects for the prevention or treatment of mild diverse breast cancer, especially given the current absence of preventive treatments.

Although our study provides valuable insights into the modulation of antitumor immunity and the TIME, there are limitations that need to be addressed. The use of murine models may not fully capture the complexity of human tumor immunology, underscoring the importance of clinical validation. A key limitation of our study is that TdLs contain not only tumor-specific antigens (TSA) but also other tumor-associated antigens (TAA) and immunostimulatory components, which could contribute to the observed antitumor immune response. While this complexity makes it challenging to attribute the entire immune response solely to neoantigen presentation, multiple studies have demonstrated that tumor lysates serve as an effective source of neoantigens [61]. Our results reinforce the notion that TdLs, despite their heterogeneity, remain a potent immunogenic platform capable of eliciting strong antitumor immune responses. Extending our findings to different cancer types and patient groups requires further validation. Notably, our observations with CT26 cells suggest that this model may also have potential for neoantigen-driven immunotherapy. Although the antitumor effects in CT26 were not as pronounced as in 4T1, the increased immune cell infiltration in the tumor microenvironment indicates that further investigation into its immunogenic

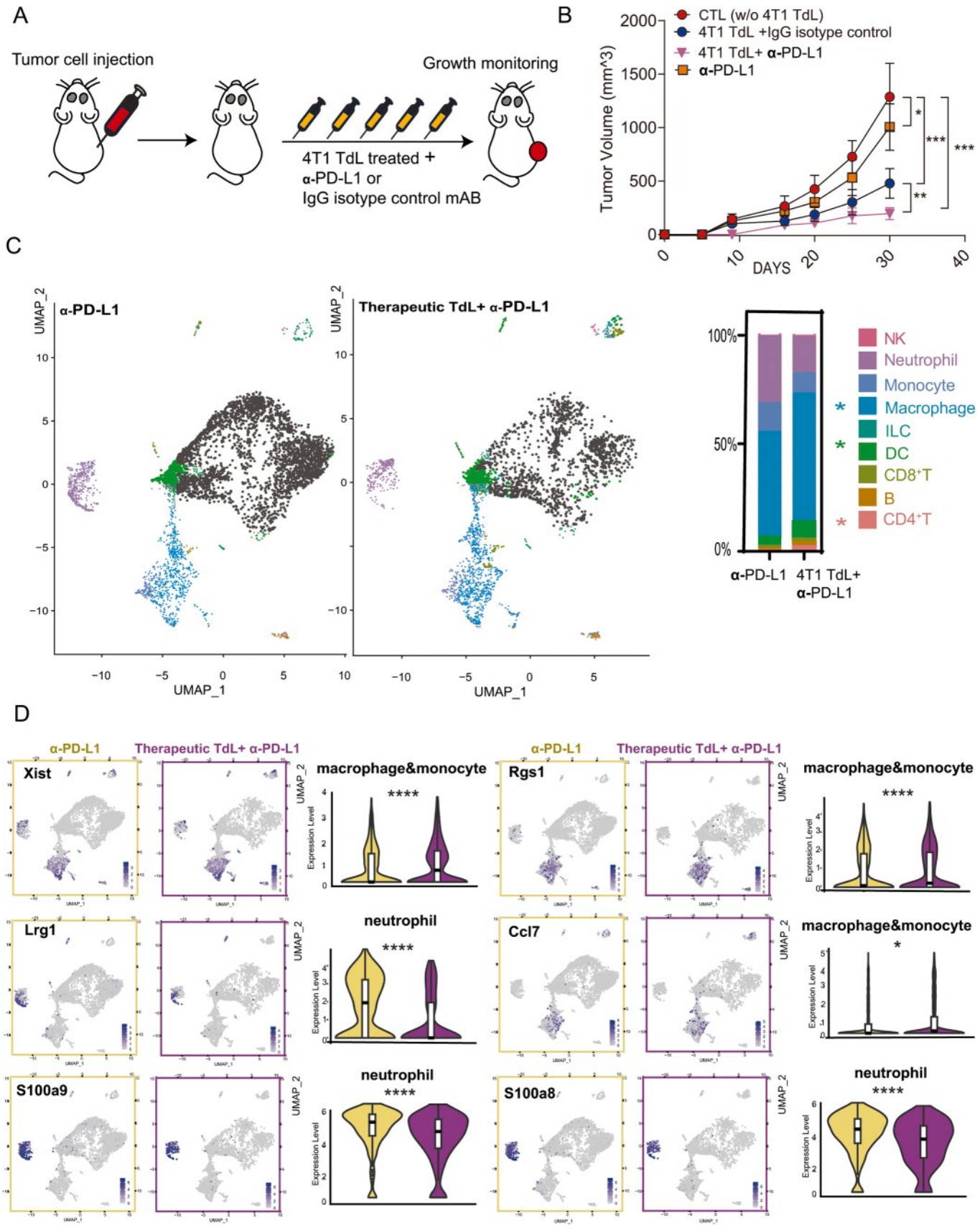

(caption on next page)

Fig. 7. Treating 4T1 syngeneic mice with both PDL1 antibody and therapeutic TdL greatly improves effectiveness. (A) Scheme of combination immunotherapy involving 4T1 TdL and an anti-PDL1 antibody, along with its control formulation, after the tumor size reached 100 mm3. (B) Tumor growth in mice with untreated CTL, 4T1 therapeutic TdL with IgG control, or anti-PDL1 antibody (n=5). Two-way ANOVA with Tukey's HSD was conducted, with statistical significance denoted by *p < 0.05, **p < 0.01 and ***p < 0.001. (C) UMAP plot illustrating the characterized cell clusters originating from tumors treated with anti-PDL1 inhibitor and 4T1 therapeutic TdL + anti-PDL1 inhibitor, encompassing natural killer (NK) cells, neutrophils, monocytes, macrophages, innate lymphoid cells (ILCs), dendritic cells (DCs), CD8+ T cells, B cells, and CD4+ T cells. Each sample was subjected to analysis for anti-PDL1 inhibitor (n=1) and 4T1 therapeutic TdL+ anti-PDL1 inhibitor (n=1), resulting in a total of 1,515 and 1584 immune cells normalized to 100%, respectively. (D) UMAP of the expression of genes such as SPARC, RGS1, XIST, CCL7, LRG1, S100A8, and S100A9 within tumor cell clusters. A violin plot of gene expression levels is displayed, with the median within the range box. Sparc is associated with the nonimmune component, whereas Rgs1, Xist, and CCl7 are associated with macrophages and monocytes. Lrg1, S100a8, and S1009 are associated with neutrophils.

properties could be promising for colorectal cancer treatment. In particular, in the case of lung metastasis, we observed both the inhibition of spontaneous lung metastasis and the same metastasis-inhibiting effect in an experimental lung metastasis model using TdLs and neoantigen peptide-loaded LNPs. Further research may lead to the discovery of genomic characteristics that drive molecular biological changes in microenvironment cells associated with lung metastasis caused by the application of therapies.

In summary, we show that novel strategies of neoantigen-based immunomodulation including the prior exposure to live tumor cells, administration of tumor lysates before and after the tumor establishment, and delivering selected neoantigens via nanoparticle can effectively inhibit tumor growth and metastasis in the mouse model of triple-negative breast cancer. These approaches significantly remodeled the tumor immune microenvironment and substantially increased the efficacy of immune checkpoint inhibitors. While the preclinical nature of and reliance on murine models in this study necessitate further validation in clinical settings, the promising results suggest that targeting tumor-specific neoantigens could lead to more effective treatments for patients with triple-negative breast cancer.

Statement of translational relevance

This study explores the potential of targeting tumor neoantigens to enhance antitumor immunity in breast cancer, an area with significant unmet clinical needs. Using a syngeneic mouse mammary carcinoma model, we demonstrate that prior exposure to tumor cells or treatment with tumor cell-derived lysates (TdLs) can significantly remodel the tumor immune microenvironment (TIME), leading to reduced tumor growth and metastasis. The findings indicate that combining neoantigen-targeting strategies with immune checkpoint inhibitors could enhance therapeutic efficacy. The development of a lipid nanoparticle (LNP)-based delivery system for neoantigen peptides further highlights a promising approach for personalized breast cancer treatment. These results underscore the potential of neoantigen-targeted therapies in clinical settings and support their continued investigation in future clinical trials for breast cancer patients.

Fig. S1. The groups pre-exposed to 4T1 cells or treated with TdLs (tumor-derived lysates) exhibited consistent 4T1 tumor inhibition in in vivo experiments. In repeated experiments, variations in various conditions for 4T1 tumors were shown to have no effect on the inhibition of 4T1 tumors by A) control treatment without poly I:C (polyinosinic-polycytidylic acid), B) treatment with poly I:C, C) the presence or absence of the combination of 4T1 TdL and poly I:C, and d) additional treatment with 4T1 MHC (major histocompatibility complex) class I+II-targeting peptides.

Significance was assessed using a two-way ANOVA (analysis of variance) with Bonferroni correction. $*p < 0.05$, $***p < 0.001$, $***p < 0.0001$, *and ns; not significant.*

Fig. S2. Flow cytometry was performed on the basis of the gating principle. The FACS (fluorescence-activated cell sorting) dot plots display sorting gates for the general immune profile, such as: PMN-MDSCs (polymorphonuclear myeloid-derived suppressor cells), Monocytes, M1 and M2 TAMs (tumor-associated macrophages), B cells, T cells, and NK cells (natural killer cells) related to tumors from mice pre-exposed to A) 4T1 cells, and B) treated with 4T1 TdL.

Fig. S3. The expression of memory T cell-related genes was upregulated in tumors in response to pre-exposure to 4T1 cells and treatment with TdL.

Fig. S4. Flow cytometry gating strategy for identifying central memory T cells (Tcm; $CD62L^{+}CD44^{+}$) and effector memory T cells (Tem; $CD62L^{-}CD44^{+}$) among tumor-infiltrating lymphocytes (TILs).

Fig. S5. Mice treated with 4T1 TdL tended to have increased numbers of effector and central memory T cells in their blood. A) Representative flow cytometry gating strategy. B) Quantified data are presented as means ± SDs (standard deviations), $n = 3$. $p < 0.05$ according to the Mann–Whitney test; *ns = not significant.*

Fig. S6. Evaluation of the effect of 4T1 TdL on a CD20-depleted mouse model.

To investigate whether the efficacy of 4T1 TdL affects the function of specific immune cells, mice were treated with three rounds of IgG (immunoglobulin G) isotype control or a neutralizing α-CD20 mAb (monoclonal antibody). Following confirmation of CD20+ B cell depletion in mouse blood (A), the prophylactic administration of 4T1 TdL inhibited tumor growth in a CD20+ B cell-depleted model. (B) Tumor growth was observed along with CD3 (cluster of differentiation 3) depletion after TdL treatment, as depicted in Fig. 5b. The same effect was observed in the CTL group (cytotoxic T lymphocyte group). The data are presented as median values ± SDs; two-way ANOVA. $*p < 0.05$, $**p < 0.01$, $***p < 0.001$, $***p < 0.0001$; *ns, not significant.*

Fig. S7. Flow cytometry data revealed that 4T1 TdL efficiently matured and activated BMDCs (bone marrow-derived dendritic cells).

Fig. S8. Intracellular flow cytometry analysis of CRTAM+ (class I-restricted T cell-associated molecule) T cells in tumors from mice pre-exposed to 4T1 cells, or treated with 4T1 TdL. The data are presented as means ± SDs, $n = 3$. $p < 0.05$ according to the Mann–Whitney test; *ns, not significant.*

Fig. S9. Therapeutic treatment with 4T1 TdL significantly inhibited 4T1 tumor growth.

Significance was assessed using a two-way ANOVA; $p < 0.0001$.

Figure S10. Flow cytometry plots illustrating sorting gates for the overall immune cell profile associated with the therapeutic application of 4T1 TdL.

Fig. S11. Intracellular flow cytometry analysis of CRTAM+ T cells in tumors therapeutically treated with 4T1 TdL. The data are presented as median values ± SDs; Mann–Whitney test. $p < 0.05$; *ns, not significant.*

Fig. S12. Mice subjected to therapeutic 4T1 TdL treatment tended to have fewer exhausted T cells. The bar graph presents flow cytometry data for: (A) Draining lymph nodes (DLNs) (B) Tumors

Fig. S13. Heatmap showing the average expression of differentially expressed genes (*-log10 adjusted p-value > 0*) plotted per cell type across various treatment conditions. The expression values were normalized by row. Genes in red: Upregulated. Genes in blue: Downregulated compared to tumors from mice treated with 4T1 TdL + α-PD-L1 mAb (programmed death-ligand 1 monoclonal antibody) relative to mice

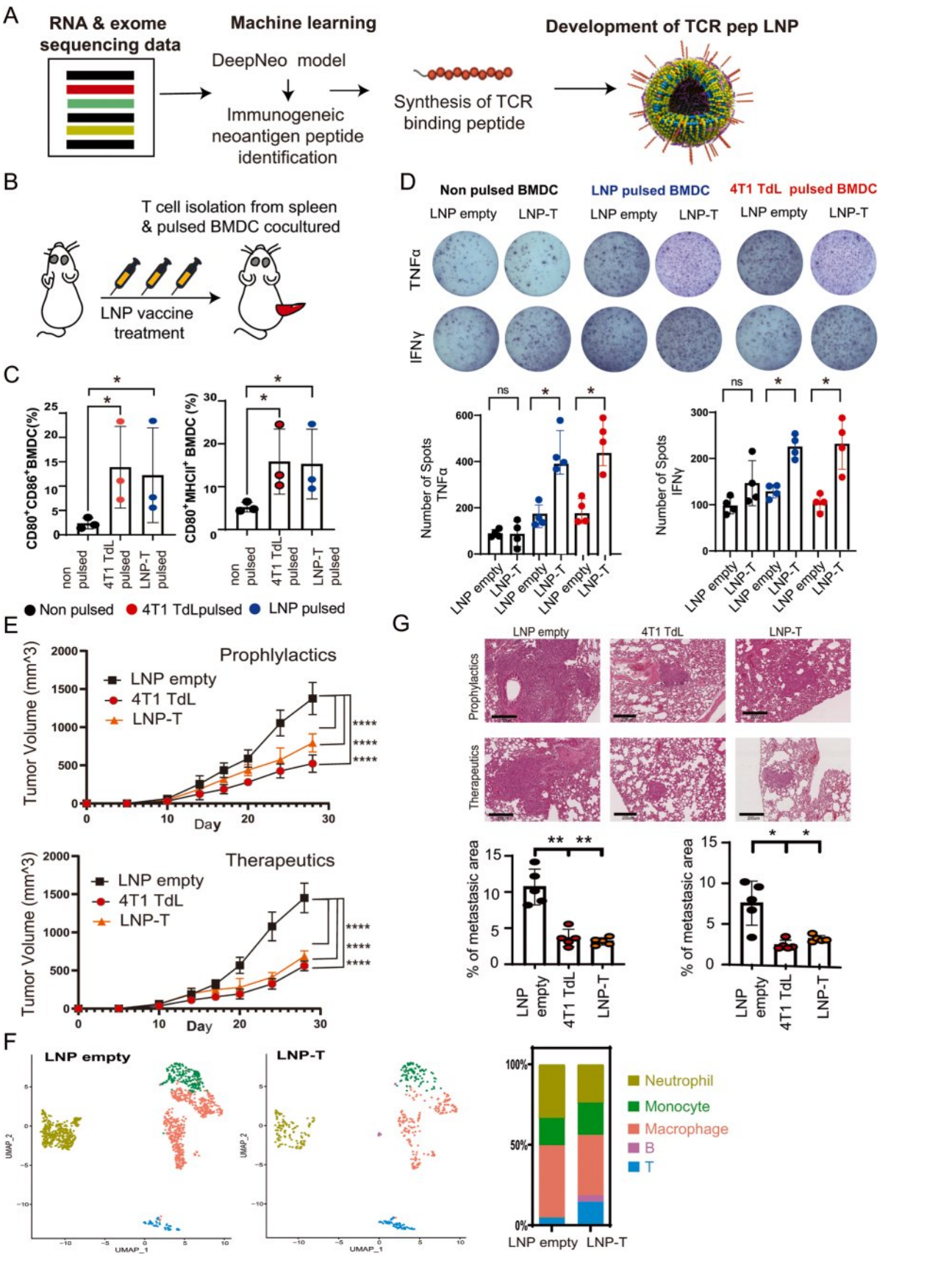

(caption on next page)

Fig. 8. Enhanced antitumor efficacy of a 4T1 neoantigen peptide loaded in LNPs. (A) The illustration depicts the process of 4T1 neoantigen prediction and LNP development. (B) This schematic shows the effective activation of dendritic cells (DCs) as antigen-presenting cells pulsed with either the neoantigen peptide-loaded LNP or 4T1 TdL via FACS analysis (C); the treatments were administered three times to the mice. (D) The levels of TNF-α and IFN-γ secreted from activated DCs cocultured with T cells isolated from the spleen of mice treated with LNPs with or without T-cell-targeting neoantigen peptide were assessed via ELISpot assays (n=3). Statistical analysis was conducted via the Mann–Whitney test, with *$p < 0.05$ indicating statistical significance and "ns" indicating not significant. Error bars were used to depict the standard error of the mean (SEM). d Monitoring of tumor growth (E) and of spontaneous lung metastasis (F) in mice were conducted for both prophylactic and therapeutic treatments, including LNP empty, 4T1 TdL, and LNP loaded with T cell-targeting peptides. Scale bar, 200 μm. Significance was assessed via two-way ANOVA with Tukey's HSD test and the Mann–Whitney test, where *$p < 0.05$, **$p < 0.01$ and ****$p < 0.0001$ denote statistical significance, and "ns" indicates not significant. (G) UMAP plot illustrating the identified cell types originating from tumors treated with empty LNPs or LNPs loaded with T cell-targeting peptides (n=1). These cell types clustered into neutrophils, monocytes, macrophages, B cells, and T cells, with a total of 1,187 and 521 cells from tumors treated with empty LNPs or LNPs loaded with T cell-targeting peptides, respectively.

treated with α-PD-L1 mAb only.

Fig. S14. Flow cytometry gating criteria for the activation of: Non-treated BMDCs, 4T1 TdL-treated BMDCs and 4T1 neoantigen peptide-loaded LNP-treated BMDCs (lipid nanoparticle-treated bone marrow-derived dendritic cells).

Declarations

Ethics approval statement

All animal experiments were conducted in accordance with ethical guidelines and were approved by the Institutional Animal Care and Use Committee (IACUC) of Seoul National University Hospital (approval number: 23-0249-S1A0).

Consent for publication

All individuals whose data are included in this manuscript have given their explicit consent for publication. This includes any individual details, images, or videos. The necessary consent forms have been obtained and are available upon request.

Availability of data and materials

The datasets generated and/or analysed during the current study, including all raw data supporting the findings presented in the figures, have been uploaded as supporting data files. These datasets are available from the corresponding author, [Hyeong-Gon Moon], upon reasonable request. Data supporting the findings of this study will be provided, subject to any privacy restrictions, and in accordance with the relevant conditions for access.

CRediT authorship contribution statement

Yujeong Her: Conceptualization, Data curation, Formal analysis, Validation, Visualization, Writing – original draft, Investigation, Methodology. **Jeong Yeon Kim:** Software, Validation, Visualization. **Hocheol Shin:** Resources. **Kwangmin Yu:** Resources. **Kyu-Jin Lee:** Resources. **Yi Rang Na:** Supervision. **Sangyong Jon:** Funding acquisition, Supervision. **Jung Kyoon Choi:** Supervision. **Hyeong-Gon Moon:** Conceptualization, Funding acquisition, Project administration, Supervision, Writing – review & editing.

Declaration of competing interest

The authors declare that they have no known competing financial interests or personal relationships that could have appeared to influence the work reported in this paper.

Acknowledgments

We would like to thank our laboratory members and collaborators for their invaluable support and insights throughout the course of this study.

Funding support

This research was supported by a grant of the Korea Health Technology R&D Project through the Korea Health Industry Development Institute (KHIDI), funded by the Ministry of Health & Welfare, Republic of Korea (grant number: HI22C0497), and by the Ministry of Trade, Industry and Energy of the Republic of Korea (grant number: RS-2024-00407561).

Supplementary materials

Supplementary material associated with this article can be found, in the online version, at doi:10.1016/j.neo.2025.101205.

References

[1] E.A. Rakha, et al., Prognostic markers in triple-negative breast cancer, Cancer 109 (2007) 25–32.
[2] A.N. Renrick, Z.T. Dunbar, A. Shanker, Update on the current revolution in cancer immunotherapy, Immunotherapy 11 (2019) 15–20.
[3] J. Tang, A. Shalabi, VM. Hubbard-Lucey, Comprehensive analysis of the clinical immuno-oncology landscape, Ann. Oncol. 29 (2018) 84–91.
[4] R.K. Vaddepally, P. Kharel, R. Pandey, R. Garje, AB. Chandra, Review of indications of FDA-approved immune checkpoint inhibitors per NCCN guidelines with the level of evidence, Cancers 12 (2020) 738.
[5] H.S. Rugo, et al., Safety and antitumor activity of pembrolizumab in patients with estrogen receptor-positive/human epidermal growth factor receptor 2-negative advanced breast cancer, Clin. Cancer Res. 24 (2018) 2804–2811.
[6] Santa-Maria CA, et al., A pilot study of durvalumab and tremelimumab and immunogenomic dynamics in metastatic breast cancer, Oncotarget 9 (2018) 18985–18996.
[7] J.J. Havel, D. Chowell, TA. Chan, The evolving landscape of biomarkers for checkpoint inhibitor immunotherapy, Nat. Rev. Cancer 19 (2019) 133–150.
[8] S.D. Brown, et al., Neo-antigens predicted by tumor genome meta-analysis correlate with increased patient survival, Genome Res 24 (2014) 743–750.
[9] B. Heemskerk, P. Kvistborg, TN. Schumacher, The cancer antigenome, EMBO J. 32 (2013) 194–203.
[10] V. Lennerz, et al., The response of autologous T cells to a human melanoma is dominated by mutated neoantigens, Proc. Natl. Acad. Sci. U. S. A. 102 (2005) 16013–16018.
[11] M.M. Gubin, M.N. Artyomov, E.R. Mardis, RD. Schreiber, Tumor neoantigens: building a framework for personalized cancer immunotherapy, J. Clin. Invest. 125 (2015) 3413–3421.
[12] J.L. Tanyi, et al., Personalized cancer vaccine effectively mobilizes antitumor T cell immunity in ovarian cancer, Sci. Transl. Med. 10 (2018) eaao5931.
[13] L. Chen, et al., Bacterial cytoplasmic membranes synergistically enhance the antitumor activity of autologous cancer vaccines, Sci. Transl. Med. 13 (2021) eabc2816.
[14] T. Wang, et al., A cancer vaccine-mediated postoperative immunotherapy for recurrent and metastatic tumors, Nat. Commun. 9 (2018) 1532.
[15] R. Piranlioglu, et al., Primary tumor-induced immunity eradicates disseminated tumor cells in syngeneic mouse model, Nat. Commun. 10 (2019) 1430.
[16] R.M. Zinkernagel, et al., Antigen localisation regulates immune responses in a dose- and time-dependent fashion: a geographical view of immune reactivity, Immunol. Rev. 156 (1997) 199–209.
[17] B.J. Masten, MF. Lipscomb, Comparison of lung dendritic cells and B cells in stimulating naive antigen-specific T cells, J. Immunol. 162 (1999) 1310–1317.
[18] L.J. Sigal, S. Crotty, R. Andino, KL. Rock, Cytotoxic T-cell immunity to virus-infected non-haematopoietic cells requires presentation of exogenous antigen, Nature 398 (1999) 77–80.
[19] S. Balan, K.J. Radford, N. Bhardwaj, Unexplored horizons of cDC1 in immunity and tolerance, Adv. Immunol. 148 (2020) 49–91.
[20] V. Mollica Poeta, M. Massara, A. Capucetti, R. Bonecchi, Chemokines and chemokine receptors: new targets for cancer immunotherapy, Front. Immunol. 10 (2019) 379.

[21] L. Belarif, et al., IL-7 receptor blockade blunts antigen-specific memory T cell responses and chronic inflammation in primates, Nat. Commun. 9 (2018) 4483.
[22] C.P. Cook, et al., A single-cell transcriptional gradient in human cutaneous memory T cells restricts Th17/Tc17 identity, Cell Rep. Med. 3 (2022) 100715.
[23] Y.S. Choi, et al., LEF-1 and TCF-1 orchestrate T(FH) differentiation by regulating differentiation circuits upstream of the transcriptional repressor Bcl6, Nat. Immunol. 16 (2015) 980–990.
[24] A.M. Hammer, G.M. Sizemore, V.C. Shukla, A. Avendano, S.T. Sizemore, J. J. Chang, R.D. Kladney, M.C. Cuitiño, K.A. Thies, Q. Verfurth, A. Chakravarti, Stromal PDGFR-α activation enhances matrix stiffness, impedes mammary ductal development, and accelerates tumor growth, Neoplasia 19 (6) (2017) 496–508.
[25] B. Li, L. Brusman, J. Dahlka, L.A. Niswander, TMEM132A ensures mouse caudal neural tube closure and regulates integrin-based mesodermal migration, Development 149 (17) (2022) dev200442 p.
[26] S. Goktas Aydin, et al., Impact of SPARC expression on treatment response of pembrolizumab and brain metastasis in patients with metastatic non-small cell lung cancer, Int. Immunopharmacol. 124 (2023) 110947.
[27] S. Zhang, et al., RGS1 and related genes as potential targets for immunotherapy in cervical cancer: computational biology and experimental validation, J. Transl. Med. 20 (2022) 334.
[28] J. Li, et al., XIST/miR-34a-5p/PDL1 axis regulated the development of lung cancer cells and the immune function of CD8(+) T cells, J. Recept. Signal Transduct. Res. 42 (2022) 469–478.
[29] M. Zhang, et al., CCL7 recruits cDC1 to promote antitumor immunity and facilitate checkpoint immunotherapy to non-small cell lung cancer, Nat. Commun. 11 (2020) 6119.
[30] M.N. O'Connor, et al., LRG1 destabilizes tumor vessels and restricts immunotherapeutic potency, Med 2 (2021) 1231–1252, e10.
[31] L.R. Begg, et al., S100A8/A9 predicts response to PIM kinase and PD-1/PD-L1 inhibition in triple-negative breast cancer mouse models, Commun. Med. 4 (2024) 22.
[32] M.K. Malhotra, LA. Emens, The evolving management of metastatic triple negative breast cancer, Semin. Oncol. 47 (2020) 229–237.
[33] J. Cortes, et al., Pembrolizumab plus chemotherapy versus placebo plus chemotherapy for previously untreated locally recurrent inoperable or metastatic triple-negative breast cancer (KEYNOTE-355): a randomised, placebo-controlled, double-blind, phase 3 clinical trial, Lancet 396 (2020) 1817–1828.
[34] P. Schmid, et al., Atezolizumab and nab-paclitaxel in advanced triple-negative breast cancer, N. Engl. J. Med. 379 (2018) 2108–2121.
[35] M. Hahn, M.J. Nicholson, J. Pyrdol, KW. Wucherpfennig, Unconventional topology of self peptide-major histocompatibility complex binding by a human autoimmune T cell receptor, Nat. Immunol. 6 (2005) 490–496.
[36] D.K. Sethi, et al., A highly tilted binding mode by a self-reactive T cell receptor results in altered engagement of peptide and MHC, J. Exp. Med. 208 (2011) 91–102.
[37] J.H. Kessler, CJ. Melief, Identification of T-cell epitopes for cancer immunotherapy, Leukemia 21 (2007) 1859–1874.
[38] V. Leko, SA. Rosenberg, Identifying and targeting human tumor antigens for T cell-based immunotherapy of solid tumors, Cancer Cell 38 (2020) 454–472.
[39] J. Bauman, et al., 798 Safety, tolerability, and immunogenicity of mRNA-4157 in combination with pembrolizumab in subjects with unresectable solid tumors (KEYNOTE-603): an update, J. Immuno. Ther. Cancer 8 (2020) A477.
[40] E. Kon, N. Ad-El, I. Hazan-Halevy, L. Stotsky-Oterin, D. Peer, Targeting cancer with mRNA-lipid nanoparticles: key considerations and future prospects, Nat. Rev. Clin. Oncol. 20 (2023) 739–754.
[41] N. van Rooij, et al., Tumor exome analysis reveals neoantigen-specific T-cell reactivity in an ipilimumab-responsive melanoma, J. Clin. Oncol. 31 (2013) e439–e442.
[42] N.S. Wilson, et al., Systemic activation of dendritic cells by toll-like receptor ligands or malaria infection impairs cross-presentation and antiviral immunity, Nat. Immunol. 7 (2006) 165–172.
[43] D.A. Wick, et al., Surveillance of the tumor mutanome by T cells during progression from primary to recurrent ovarian cancer, Clin. Cancer Res. 20 (2014) 1125–1134.
[44] E. Tran, et al., Cancer immunotherapy based on mutation-specific CD4+ T cells in a patient with epithelial cancer, Science 344 (2014) 641–645.
[45] B. Pellegrino, et al., Luminal breast cancer: risk of recurrence and tumor-associated immune suppression, Mol. Diagn. Ther. 25 (2021) 409–424.
[46] J. Galon, et al., Type, density, and location of immune cells within human colorectal tumors predict clinical outcome, Science 313 (2006) 1960–1964.
[47] G.R. Weiss, et al., Molecular insights on the peripheral and intratumoral effects of systemic high-dose rIL-2 (aldesleukin) administration for the treatment of metastatic melanoma, Clin. Cancer Res. 17 (2011) 7440–7450.
[48] J.L. Messina, et al., 12-Chemokine gene signature identifies lymph node-like structures in melanoma: potential for patient selection for immunotherapy? Sci. Rep. 2 (2012) 765.
[49] B. Virassamy, et al., Intratumoral CD8(+) T cells with a tissue-resident memory phenotype mediate local immunity and immune checkpoint responses in breast cancer, Cancer Cell 41 (2023) 585–601, e8.
[50] N.B. Jamieson, AV. Maker, Gene-expression profiling to predict responsiveness to immunotherapy, Cancer Gene Ther 24 (2017) 134–140.
[51] T.D. de Gruijl, A.J. van den Eertwegh, H.M. Pinedo, RJ. Scheper, Whole-cell cancer vaccination: from autologous to allogeneic tumor- and dendritic cell-based vaccines, Cancer Immunol. Immunother. 57 (2008) 1569–1577.
[52] N. Pardi, M.J. Hogan, F.W. Porter, Weissman D. mRNA vaccines - a new era in vaccinology, Nat. Rev. Drug Discov. 17 (2018) 261–279.
[53] F. Saade, N. Petrovsky, Technologies for enhanced efficacy of DNA vaccines, Expert Rev. Vaccines 11 (2012) 189–209.
[54] S. Gross, et al., Short peptide vaccine induces CD4+ T helper cells in patients with different solid cancers, Cancer Immunol. Res. 4 (2016) 18–25.
[55] L.B. Alexandrov, et al., Signatures of mutational processes in human cancer, Nature 500 (2013) 415–421.
[56] J. Pol, G. Kroemer, L. Galluzzi, First oncolytic virus approved for melanoma immunotherapy, Oncoimmunology 5 (2016) e1115641.
[57] M.A. Cheever, CS. Higano, PROVENGE (Sipuleucel-T) in prostate cancer: the first FDA-approved therapeutic cancer vaccine, Clin. Cancer Res. 17 (2011) 3520–3526.
[58] U. Dafni, et al., Efficacy of cancer vaccines in selected gynaecological breast and ovarian cancers: a 20-year systematic review and meta-analysis, Eur. J. Cancer 142 (2021) 63–82.
[59] F.E. González, A. Gleisner, F. Falcón-Beas, F. Osorio, M.N. López, F. Salazar-Onfray, Tumor cell lysates as immunogenic sources for cancer vaccine design, Human Vacci. Immunotherapeut. 10 (11) (2014) 3261–3269, pp.
[60] C. Lhuillier, N.P. Rudqvist, T. Yamazaki, T. Zhang, M. Charpentier, L. Galluzzi, N. Dephoure, C.C. Clement, L. Santambrogio, X.K. Zhou, S.C. Formenti, Radiotherapy-exposed CD8+ and CD4+ neoantigens enhance tumor control, J. Clin. Invest. 131 (5) (2021).
[61] M.O. Mohsen, D.E. Speiser, J. Michaux, H. Pak, B.J. Stevenson, M. Vogel, V. P. Inchakalody, S. de Brot, S. Dermime, G. Coukos, M. Bassani-Sternberg, Bedside formulation of a personalized multi-neoantigen vaccine against mammary carcinoma, J. Immunother. Cancer 10 (1) (2022) e002927.